Influence of Natural Fractures on Tight Oil Migration and Production: A Case Study of Permian Lucaogou Formation in Jimsar Sag, Junggar Basin, NW China

Yunzhao Zhang[1,2], **Lianbo Zeng**[*1,2], **Qun Luo**[*1,3], **Rukai Zhu**[4,5,6], **Wenya Lyu**[1,2],
Dongdong Liu[1,3], **Quanqi Dai**[1,2], **Shouxu Pan**[7]

1. *State Key Laboratory of Petroleum Resources and Prospecting, China University of Petroleum, Beijing* 102249, *China*
2. *College of Geosciences, China University of Petroleum, Beijing* 102249, *China*
3. *Unconventional Petroleum Research Institute, China University of Petroleum, Beijing* 102249, *China*
4. *Research Institute of Petroleum Exploration and Development, CNPC, Beijing* 100083, *China*
5. *Key Laboratory of Oil and Gas Reservoirs, CNPC, Beijing* 100083, *China*
6. *National Energy Tight Oil and Gas R&D Center, Beijing* 100083, *China*
7. *School of Geosciences, China University of Petroleum, Qingdao* 266580, *China*

Yunzhao Zhang: https://orcid.org/0000-0003-3883-5022; Lianbo Zeng: https://orcid.org/0000-0002-6470-8206;
Qun Luo: https://orcid.org/0000-0001-9639-8401

ABSTRACT: Natural fractures, as the main flow channels and important storage spaces, have significant effects on the migration, distribution, and accumulation of tight oil. According to outcrop, core, formation micro image (FMI), cast-thin-section, and scanning electron microscopy data from the tight reservoir within the Permian Lucaogou Formation of the Junggar Basin, tectonic fractures are prevalent in this formation mainly on micro to large scale. There are two types of fractures worth noticing: diagenetic fractures and overpressure-related fractures, primarily at micro to medium scale. The diagenetic fractures consist of bedding fractures, stylolites, intragranular fractures, grain-boundary fractures, and diagenetic shrinkage fractures. Through FMI interpretation and Monte Carlo method evaluation, the macro-fractures could be considered as migration channels, and the micro-fractures as larger pore throats that function as storage spaces. The bedding fractures formed earlier than all tectonic fractures, while the overpressure-related fractures formed in the Middle and Late Jurassic. The bedding fractures and stylolites function as the primary channels for horizontal migration of tight oil. The tectonic fractures can provide vertical migration channels and reservoir spaces for tight oil, and readjust the tight oil distribution. The overpressure-related fractures are fully filled with calcite, and hence, have little effect on hydrocarbon migration and storage capacity. The data on tight oil production shows that the density and aperture of fractures jointly determine the productivity of a tight reservoir.
KEY WORDS: natural fractures, tight reservoir, oil migration and production, Permian Lucaogou Formation, Junggar Basin.

0 INTRODUCTION

Shale gas and tight oil are increasingly becoming important targets of exploration and development worldwide (Mahmoud et al., 2020; Zhou et al., 2019; McGlade, 2012). Tight oil is expected to be explored and used in China for a prolonged time in the future (Tang et al., 2019). The majority of the literature defines tight oil as the oil preserved in reservoirs with an overburden matrix permeability less than or equal to 0.1 mD (air

permeability <1 mD) (Zou et al., 2019; Han et al., 2017). China has rich tight oil reserves and estimates of its recoverable resources range from 35×10^8 to 40×10^8 t (Pang et al., 2012; Zou et al., 2012). The Permian Lucaogou Formation in the Junggar Basin is a major target for the exploitation and development of tight oil in China (Guo et al., 2019; Zhu et al., 2019). To date, more than 7 B bbl of proven oil reserves have been determined within the Lucaogou Formation, exhibiting excellent potential for oil production (Jia et al., 2012).

Owing to the complexity of tectonic movement and diagenesis (Zeng et al., 2008b, 2007), tight oil reservoirs are usually characterized by small pores, fine throats, poor throat connectivity, and strong heterogeneity. Fractures can accumulate fluid within tight sandstone reservoirs and function as percolation channels (Zeng et al., 2013). Not only do fractures connect individual pores and improve permeability (Ozkan et al., 2011;

Laubach, 2003), they also determine the distribution of oil and gas reservoirs (Olson et al., 2010; Sava and Mavko, 2007). Fractures have become an important research focus in exploring unconventional resources and in evaluating the effectiveness of reservoir space and main migration channels (Ju et al., 2017; Nelson, 2009). There is currently an uncertainty in the attributes of subsurface natural fractures (Laubach et al., 2019), and understanding these is of great significance for the optimal design and successful enhancement of oil recovery operations (Zhao et al., 2017; Laubach et al., 2010).

Fractures can be divided into large-scale fractures (with heights >2 m and lengths >10 m), medium- and small-scale fractures (with average height <1.4 m and average length <10 m), and microscale fractures (apertures usually <10 μm) (Zeng et al., 2010a). Scientists have used petrology and mineralogy, logging, rock mechanics and acoustic experiments, seismic detection, and mathematical simulations to obtain data of fracture attributes (occurrence, density, aperture, permeability, and porosity) and have developed methods to quantitatively characterize fractures (Wang et al., 2015; Hennings, 2009; Olson et al., 2009; Prioul et al., 2007). The core, formation micro image (FMI), and cast-thin-section fracture observations are incomplete, and the subsurface fracture patterns (regarded as key attributes to constrain the fracture length distribution) cannot be determined owing to the narrow dimensions of a rock sample (Laubach et al., 2019; Olson et al., 2009; Wu and Pollard, 2002). Outcrops are often used to supplement the subsurface fracture analysis and provide an opportunity for comprehensive observations of the fracture network geometry in at least two dimensions (Ghosh et al., 2018; Hennings et al., 2000). Outcrops are typically surveyed by direct visual observations and with magnifying lenses. Truncation occurs typically because of the difficulty of measuring small fractures (<0.05 mm) (Santos et al., 2015). In terms of predicting the fracture distribution, various techniques have been put forward, including geological analysis, structural curvature analysis, longitudinal wave anisotropy analysis, and tectonic stress field simulations (Ju et al., 2019; Liu et al., 2018; Wang et al., 2017; Wei and Anand, 2008). Although the research methods and the theory of reservoir fractures have made noticeable progress, the evaluation of reservoir fractures is undoubtedly an essential and challenging aspect of evaluating tight resources (Zeng et al., 2013; Olson et al., 2009).

Some scientists have researched the characteristics, controlling factors, genetic mechanisms, formation stages, and logging identifiers of natural fractures in the Junggar Basin (Zhang et al., 2020, 2018; Liu D D et al., 2019). However, fracture types and characteristics governing the migration and charging of tight oil, are poorly understood in the Lucaogou Formation. The classification, characteristics, and formation time of natural fractures and their contribution to tight reservoirs are the key information for investigating the function of these fractures. In this study, we first described the fracture types and their characteristics within the tight sandstone based on the outcrop, core, FMI, cast-thin-section, and scanning electron microscopy (SEM) data. Next, we calculated the porosity and permeability of the different types of target fractures and analyzed the contribution of fracture porosity and permeability to the tight reservoir. Finally, we determined the formation time of natural fractures via carbon and oxygen isotope analysis on calcite filling in the veins. Using burial history, diagenetic evolution, and porosity evolution, we determined the forming time of fractures related to hydrocarbon generation and migration, and evaluated the contribution of the fractures to the charging, migration, and production of tight oil.

1 GENERAL SETTING

1.1 Location and Structure

The Junggar Basin, located in northwestern China, is a large intracontinental superimposed basin (Zhao et al., 2019). It has experienced multi-stage tectonic movements, including the Hercynian, Indosinian, Yanshan, and Himalayan movements, and has generated four regional unconformity contacts. The Jimsar sag is located in the southeast part of the Junggar Basin. The dip angle of the strata is between 3º and 5º. It is adjacent to the Jimsar fault in the north, Santai fault in the south, Laozhuangwan and Xidi faults in the west, and Qitai Bulge in the east covering an area of 1 278 km² (Fig. 1). The four tectonic stages are dominated by uplift in the east and by subsidence in the west of the sag (Yang et al., 2017; Fang et al., 2007): (1) in the Early Permian, the sag was connected with the Fukang sag and the Bogeda Piedmont sag, and became independent because of the strong tectonic subsidence during the Middle Permian; (2) during the Late Triassic, the eastern part of the sag was strongly uplifted compared with the western region, causing erosion of the Permian and Triassic formations in the east; (3) from the Cretaceous to the Cenozoic, the southeastern part of the sag was strongly uplifted, causing erosion of the Cretaceous strata; and (4) during the Cenozoic, the sag was tilted from east to west because of the forward thrusting of the Bogeda Mountains.

1.2 Strata Characterization

The Permian strata in the Jimsar sag can be divided into three formations, which the Jingjingzigou, Lucaogou, and Wutonggou formations from bottom to top (Fig. 1). The Lucaogou Formation, which is the focus of this study, is currently buried at a depth of 2 500–4 255 m. The formation is primarily composed of lacustrine and carbonate facies, deposited from a saline lake environment formed after the closure of a residual sea (Kuang et al., 2012). The Lucaogou Formation is distributed throughout the sag, thinning from southeast to northwest, with average local thicknesses 200–350 m (Fig. 2). With the regional maximum flooding surface as a reference, it can be divided into a lower member (P_2l_1) and an upper member (P_2l_2) (Kuang et al., 2013). Two sweet spots with a generally lower matrix permeability and higher hydrocarbon-bearing potential are distributed in the upper and lower parts of both the P_2l_1 and P_2l_2 of the Lucaogou Formation, named the upper (sweet spot) interval and lower (sweet spot) interval, respectively (Yang et al., 2015). The upper "sweet spot" lies in the east slope of the sag (13.3–43.0 m thick), mainly consisting of gray dolomite and feldspar lithic sandstone, sometimes coupled with gray mudstone and dolomitic mudstone. The lower "sweet spot" (17.5–67.5 m thick) consists of silty dolomite, argillaceous siltstone with lime mudstone, dolomitic mudstones, and fewer of carbonaceous mudstones. The study area, the thickness of which is more than 200 m, covers approximately 806 km². The total organic carbon content of the mudstone is 0.84% to 9.89% (average 3.49%). The chloroform bitumen "A" content ranges from 0.44% to 0.73%,
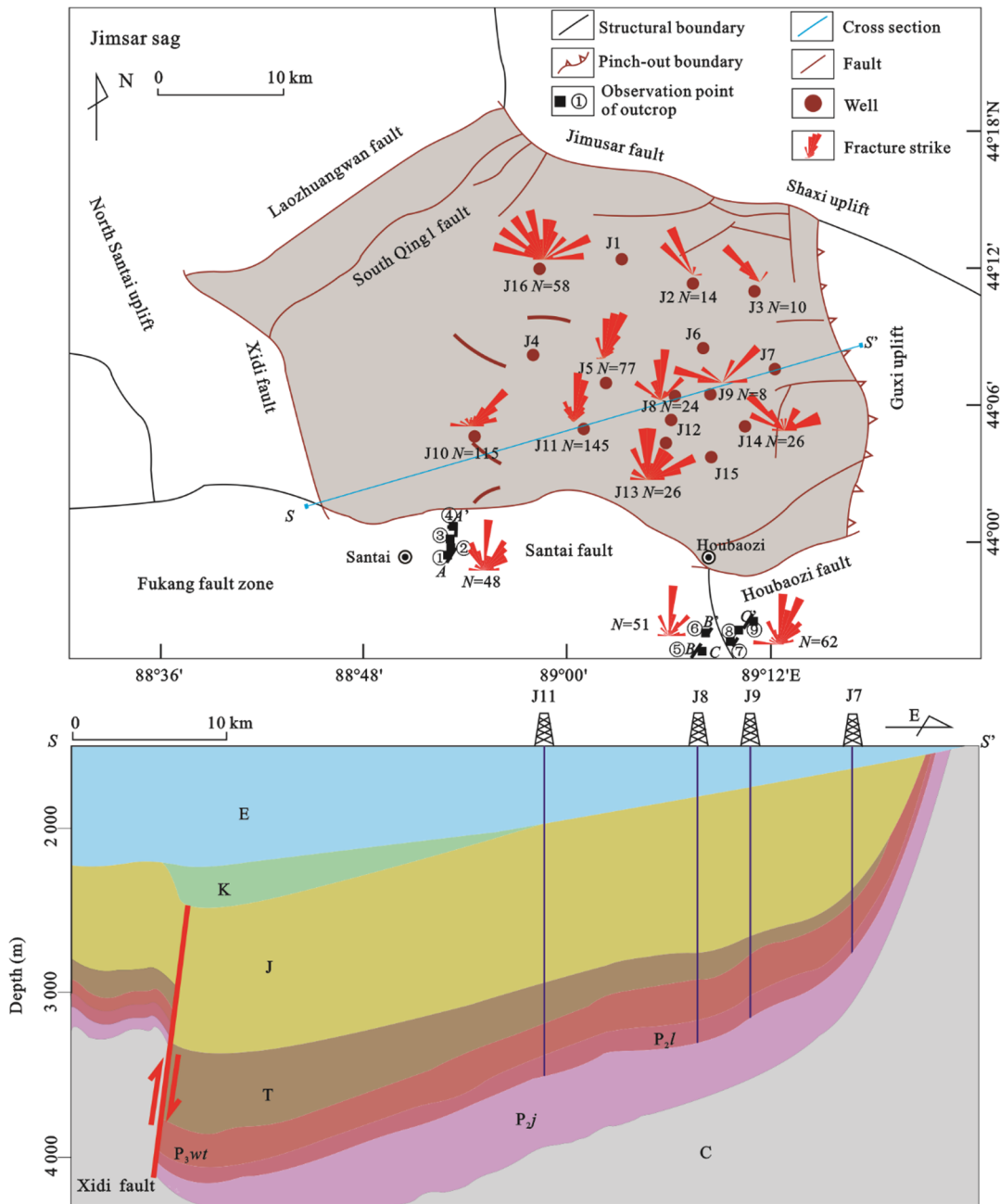
Figure 1. Locations of the study area and main wells in Jimsar sag (modified after Wu et al., 2016). The rose diagrams show the orientations of natural fractures in the tight reservoirs of the Lucaogou Formation. Section *S–S'* shows the stratigraphic structure of Jimsar sag. C. Cambrian; P_2j. Permian Jingjingzigou Formation; P_2l. Permian Lucaogou Formation; P_3wt. Permian Wutonggou Formation; T. Triassic; J. Jurassic; K. Cretaceous; E. Paleocene.

and the rock pyrolysis hydrocarbon generation potential (S1+S2) content varies from 3.50 to 20.98 mg/g. The type of organic matter is mainly – ₁ (Pang et al., 2019; Bai et al., 2017). The degree of thermal evolution of the organic matter is relatively high and reaches the Late Triassic oil window, with random vitrinite reflectance (*R*o) varying in the range of 0.7%–1.0% (Cao et al., 2017). Overall, the area is characterized by source-reservoir integration, source-proximal accumulation, and vertical distribution of oil (Jia et al., 2012; Kuang et al., 2012).

1.3   Reservoir Characterization

The tight reservoir lithology includes mudstone, sandstone, and dolomite (Kuang et al., 2013). The porosity ranges from 0.40% to 27.41%, with an average of 7.20%. The air permeability is mainly <1.0 mD, and the *in-situ* permeability is <0.1 mD in most cases. The storage spaces primary consist of intergranular pores, primary inter-crystalline pores, secondary dissolved pores, organic pores, mineral pores, and microfractures (Xi et al., 2015b). Dissolution pores account for 44% among all pores, followed by intragranular pores and intergranular pores, accounting for 26% and 22%, respectively. Nano-scale pore throats account for approximately 97% of all pore throats and represent the main tight oil storage space. The pore throat radius is mainly distributed between 50–500 nm, accounting for approximately 78% of all (Qiu et al., 2016b). The low correlation between porosity and permeability of conventional gas indicates that the micro-

fractures in tight reservoirs contribute to the reservoir space and seepage characteristics (Zha et al., 2017). Additionally, a considerable number of mineral pores are partially or fully infilled with bitumen (Su et al., 2018). Therefore, the Permian Lucaogou Formation is a typical tight reservoir, which is generally characterized by low porosity, low permeability, and strong heterogeneity.
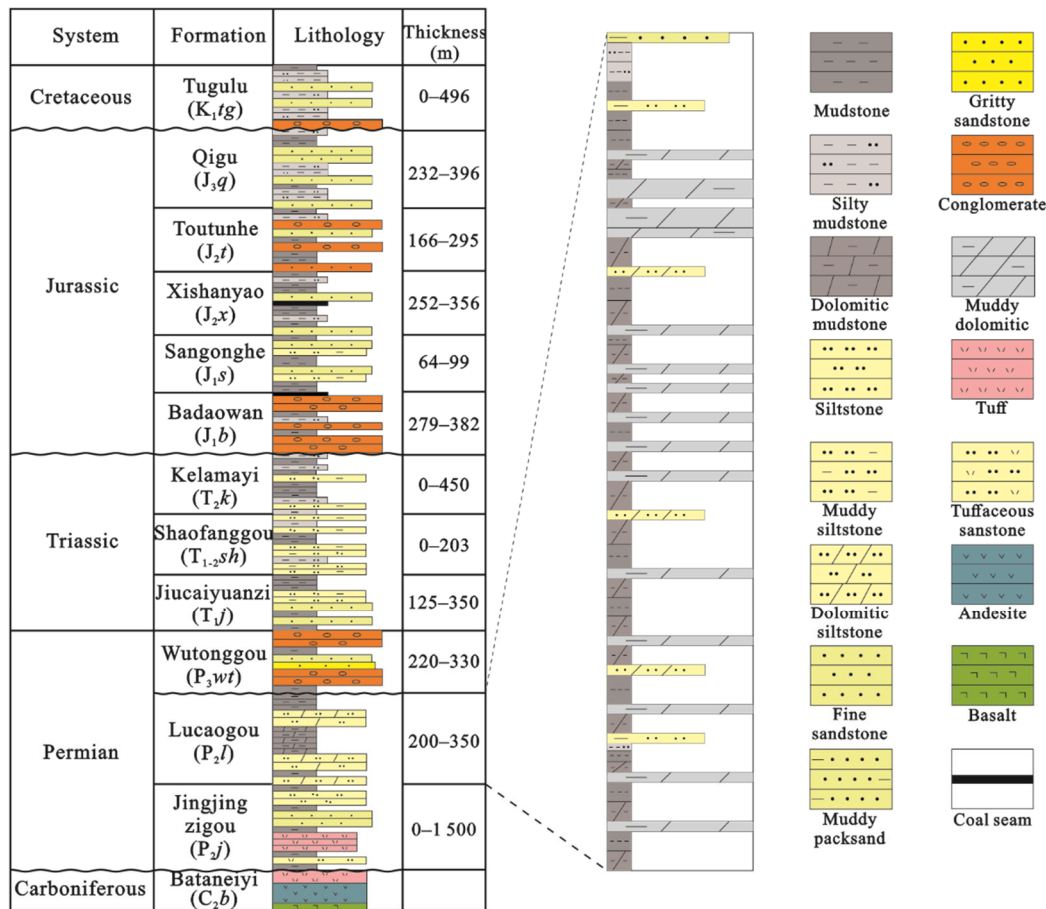

Figure 2. Stratigraphic column of the Lucaogou Formation in Jimsar sag (modified after Liu C et al., 2019; Luo et al., 2007).

Table 1 Summary of the research materials

Materials types		Core (m)	FMI (m)	Cast thin section	SEM	Hydrocarbon production
Well	J1	9.00		2		
	J2	2.70	163.12	2		√
	J3	1.10	107.34			
	J4	32.15		11	36	√
	J5	26.29	143.39			
	J6	2.75		17	13	
	J7	1.23				
	J8	241.51	243.01	67	59	√
	J9	3.23	82.51	7	6	
	J10	15.68	283	10		
	J11	112.68	171.3	39	3	
	J12	1.31		7		
	J13	24.52	92.61	8		√
	J14	5.22	94.93	23	19	
	J15	33.06				
	J16	15.49	237.03	16		√
Outcrop	A–A'	Dalongkou Reservoir section			Coordinates: 43º59'13.8"N, 88º53'09.1"E	
	B–B'	Xiaolongkou Village section			Coordinates: 43º53'26.6"N, 89º07'53.0"E	
	C–C'	Dalongkou Village section			Coordinates: 43º54'09.5"N, 89º10'46.1"E	

2 MATERIALS AND METHODS

2.1 Materials for Fracture Research

From these areas, we collected 527.92 m of cores, 209 cast thin sections from 12 wells, 130 samples for SEM from 6 wells, and 1 618.24 m of FMI logs from 10 wells (Table 1). The fracture characterization was carried out based on three outcrops at the Dalongkou Reservoir, Xiaolongkou Village, and in the fields of Dalongkou Village. We calculated the fracture porosities and permeability from 339 samples of thin sections using the Monte Carlo method and from interpretations of the FMI logs from 10 wells. The influence of natural fractures on productivity was analyzed using the hydrocarbon production data of 5 wells.

2.2 Calculation of Fracture Parameters

The outcrop of the Lucaogou Formation is widely exposed in the southeast part of the Junggar Basin. The fracture orientation (strike and dip angle) and length measurements were collected from three outcrop sections. Critical parameters such as fracture length, density, dip angle, and aperture were measured by metric-scale, feeler gauge, and protractor based on core observations. Natural and induced fractures can be discerned by the appearance of fillings on the fracture surface. The types of filling within the fractures were preliminarily identified using dilute hydrochloric acid. The petroleum logging tools for FMI included four-arm eight-electrode plates and 192 color codes for graphite electrode measurements and adjusting electrical resistivity (Lai et al., 2018). FMI can identify fractures based on the anisotropy of strata and variations in the electrical resistivity (Prioul and Jocker, 2009; Ameen and Hailwood, 2008). Owing to a large number of button electrodes and the small spacing between them, separate images of fractures can be obtained with key quantitative parameters including fracture type, fracture occurrence (strike and dip angle), fracture length (FVTL), fracture aperture (FVA), fracture density (FVDC), and fracture porosity (FVPA) (Khoshbakht et al., 2012; Lai et al., 2017). FVTL also represents the areal fracture density used by some researchers (Lai et al., 2018).

Microfractures are useful because they are more abundant than the associated macrofractures, and microfracture populations can be used for assessing fracture abundance (Anders et al., 2014; Laubach, 1989). After fractures were described by using data from cores, cast thin section (50I-P100-L, Nikon) and SEM (S4800, Hitachi) observations were conducted. The aperture of a microfracture should be measured on a thin section perpendicular to the fracture plane, while in reality, the grinding of a thin section is not always perpendicular to the fracture. Thus, the aperture of the same microfracture can vary in different parts. Moreover, even under a microscope, there are some invisible apertures. To overcome this issue, the same aperture was measured multiple times, and the average value was taken to reduce error. Later, an empirical formula was applied to revise the results (Zeng et al., 2010b).

$$e_1 = \frac{1}{n}\sum_{i=1}^{n} e_i$$

$$e = \frac{2}{\pi} e_1$$

where, e_i stands for the aperture value of the i-th part of the fracture and e_1 stands for the aperture value in the actual measurement of the fracture under the microscope.

The fracture porosity and permeability can be calculated using the Monte Carlo approximation method, based on the fracture parameters of a significant number of samples with different distribution probabilities (Howard and Nolen-Hoeksema, 1990). The application of this method has been validated in identifying low-quality fractured reservoirs (i.e., those with average fracture porosity <0.1%) (Lyu et al., 2017; Zeng et al., 2008a). The formula for calculating the fracture porosity and permeability of the sample is as follows (Zeng et al., 2010b)

$$\emptyset_f = \left(\frac{1}{A_s}\right)\sum_{i=1}^{n} L_i \cdot e_i$$

$$K_f = C \cdot \frac{1}{A_s} \cdot \sum_{i=1}^{n} e_i^3 \cdot L_i$$

where, $\emptyset_f$ is the fracture porosity; L_i is the fracture length; e_i is the fracture aperture; A_s is the sample area; K_f is the fracture permeability; and C is the proportionality coefficient. The value of C differs owing to differences in the distribution of the fractures in the sample (Zeng, 2010).

2.3 Calculation of Fracture Formation Time

Natural fractures in a reservoir generally feature multi-stage fillings, because during different stages, liquids can flow through the fractures, leaving some mineral residue or dissolving some host minerals, finally forming new minerals on walls of fractures (Fall et al., 2012; Becker et al., 2010). The veins formed in a reservoir fracture can effectively record fluid movement (Caja et al., 2006; Evans and Battles, 1999). Stable isotopes of carbon (δ^{13}C) and oxygen (δ^{18}O) of calcite were used to obtain the temperature and salinity of the fluid media (Al-Aasm et al., 1995). According to an isotopic temperature-testing equation, the test value of δ^{18}O was used to calculate the formation temperature of minerals (Giletti, 1986). Fracture cement deposits and veins could be tied to the diagenetic cement sequences with known ages, and thus an insight into the timing of fracture formation could be gained (Perez and Boles, 2004; Laubach, 1988).

3 RESULTS

3.1 Types and Characteristics of Natural Fractures

Based on the results from outcrops, cores, cast thin sections, and SEM, the natural fractures that in the Lucaogou Formation include tectonic, diagenetic, and overpressure-related fractures (Figs. 3 and 4).

3.1.1 Tectonic fractures

Tectonic fractures are related to tectonic processes and are generated in different tectonic environments and evolution stages (Ju and Sun, 2016). Crude oil can exude through the tectonic fractures (Figs. 3a and 3d). Tectonic shear fractures, accounting for the majority of fractures in the study area, formed under different tectonic stress fields, commonly featuring a high dip angle (Fig. 3b). During the formation of tectonic fractures, the direction of the fracture was parallel or vertical to that of the

fracture plane, which was straight and smooth. Structural phenomena such as striations and steps appear on the tectonic fracture plane, and its displacement could be observed (Figs. 3c, 3d, 4a, and 4f). These fractures are present in different types of lithology and exhibit an evident orientation and regular distribution. Generally, the density of tectonic fractures in dolomite, limestone, and sandstone is always higher than that in mudstone (Gong et al., 2017). Rocks with more brittle minerals (such as dolomite and calcite), finer grain size, and better assortment are easily fractured. Tectonic fractures in the dolomite, limestone, and siltstone are the most developed, followed by those in fine-grained sandstones, whereas the fracture density of mudstones is the lowest (Fig. 5a). The statistical results of the field outcrop and FMI reveal the occurrence of tectonic fractures in the study area. Four groups of tectonic fractures were found trending in the directions N-S, NNE, NE, and NNW (Figs. 1c, 6, and 7).
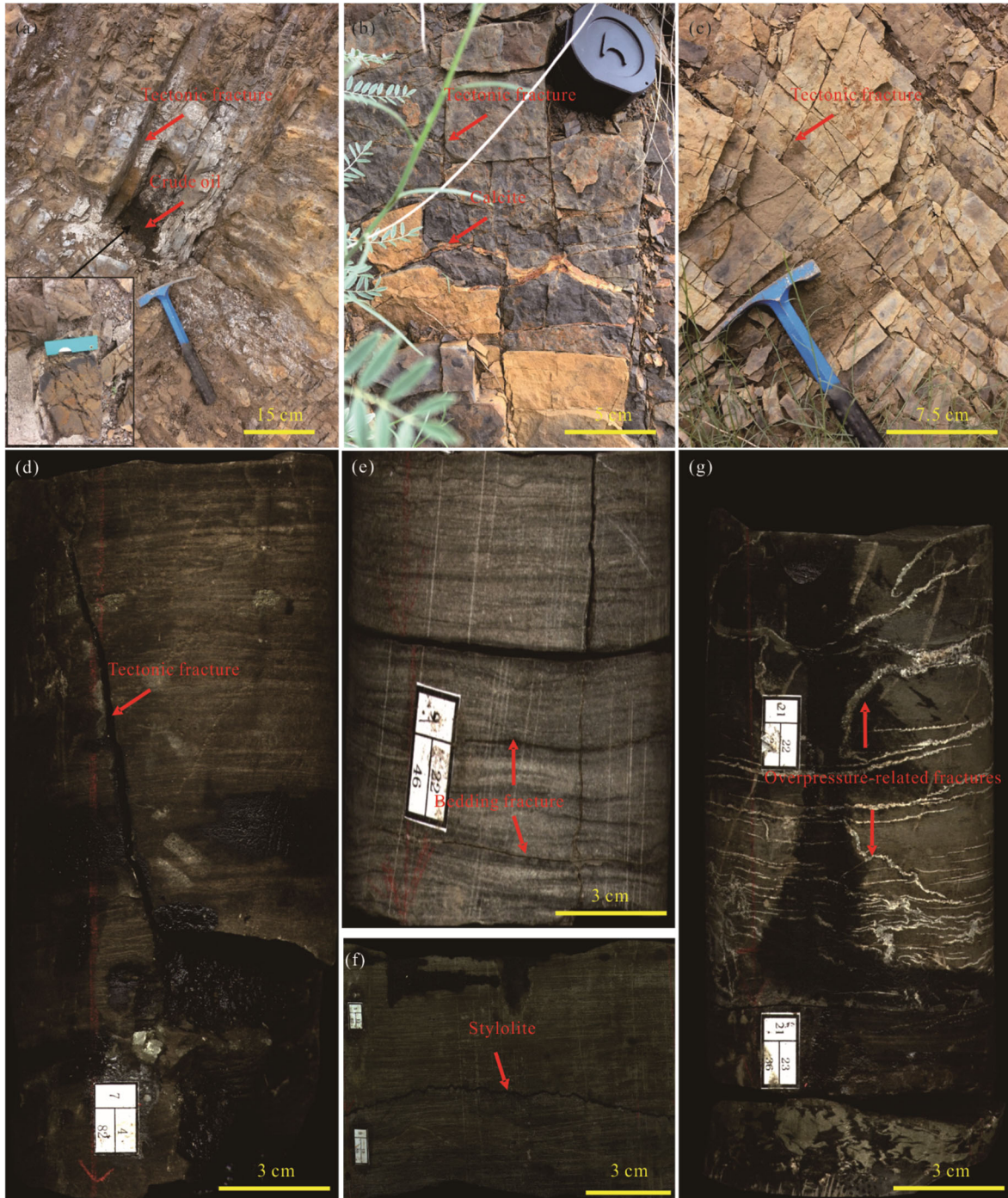

Figure 3. The photos of outcrops and cores of different types of natural fractures. The location of the well can be seen in Fig. 1. (a) Tectonic fractures and crude oil in the sandstone of the Dalongkou Reservoir section; (b) tectonic fractures in the sandstone of the Dalongkou Village section; (c) tectonic fractures in the sandstone of the Xiaolongkou Village section; (d) tectonic fractures in the siltstone of Well J11, with a depth of 3 759.99–3 760.12 m; (e) bedding fractures in the mudstone of Well J8, with a depth of 3 159.63–3 159.80 m; (f) stylolite in the siltstone of Well J5, with a depth of 3 725.88–3 726.06 m; (g) the overpressure-related fractures were filled with calcite in the limestone mudstone of Well J8, with a depth of 3 254.38–3 254.46 m.
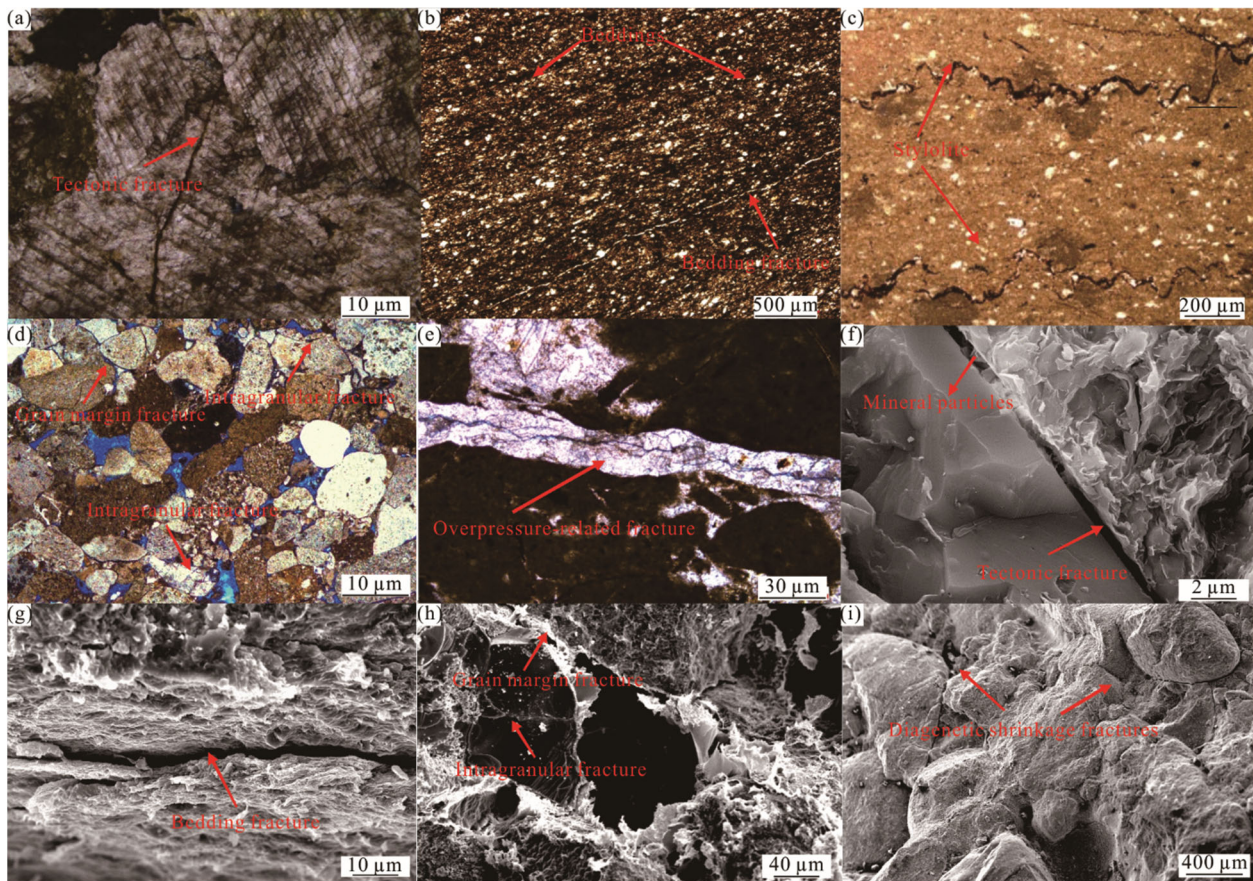
Figure 4. Pictures of showing the microfractures, the location of the well can be found in Fig. 1. (a) The tectonic microfracture in the cast thin section of fine sandstone is located in Well J11, with a depth of 3 754.20 m. The fracture passes through the horizontal beddings, and both sides of the fracture that function as the migration channel were dissolved in the process of oil filling. (b) In the cast thin section of siltstone, diagenetic fractures are located in Well J11, at a depth of 3 784.84 m. (c) In the cast thin section of argillaceous limestone, stylolite is located in Well J8, with a depth of 3 243.34 m. (d) Intragranular fracture and grain margin fractures in the cast thin section of sandy conglomerate are located in Well J8, at a depth of 3 046.58 m. (e) The overpressure-related fractures and tectonic fractures in the cast thin section of dolomitic mudstone are located in Well J11, with a depth of 3 754.69 m. The overpressure-related fractures are fully filled with calcite, and in the later stage, the tectonic fractures formed along with the overpressure-related fractures after being transformed by tectonic movement. (f) Tectonic microfractures in limestone under SEM are located in Well J8, at a depth of 3 329.68 m; a tectonic fracture is partially filled with mineral particles. (g) Bedding microfracture in mudstone under SEM is located in Well J8, at a depth of 3 398.11m. (h) In the SEM, intragranular fracture and grain margin fractures of fine sandstone are located in Well J9 with a depth of 2 853.90 m. (i) The diagenetic shrinkage fracture in the SEM of the sandy conglomerate is located in Well J8, at a depth of 3 046.58 m.

The distribution of natural fractures was dominated by mechanical stratigraphy (Gross and Eyal, 2007). They appear in the inner part of the strata and end on the lithology interface (Laubach et al., 2009). In a certain range of bed thickness, the average distance of tectonic fractures increased linearly with an increase in the bed thickness (Fig. 5b) (R^2=0.956 7). When the thickness of a single stratum was between 0 and 120 cm, most tectonic fractures developed; when it was between 120 and 200 cm, tectonic fractures were less developed, and when it was greater than 200 cm, no tectonic fracture could be found. The length of all fracture was always less than 40 cm (Fig. 8c), reflecting that fractures mostly developed within the bed thickness.

3.1.2 Diagenetic fractures

Diagenetic fractures refer to the natural fractures caused by compaction and pressure in the process of diagenesis (Zeng, 2008), including bedding, stylolite, intragranular, grain-boundary, and diagenetic shrinkage fractures. Bedding fractures account for most diagenetic fractures and are usually distributed along bedding plane. These are always interrupted, bent, wedged-out, combined, or branched, with its dip angle parallel to the bedding plane (Figs. 3e, 4b and 4g). Stylolite is a kind of planar structure that accommodates localized contractional strain (Figs. 3f and 4c), usually appearing as serrations along bedding surfaces (Bruna et al., 2019). Most of them are filled with carbonaceous clay (Fig. 3e). There are diagenetic fractures associated with and somewhat coincident with the grain-boundary, namely, intragranular and grain-boundary fractures (Figs. 4d and 4h). Intragranular fractures, lying completely within the grain, include fractures within calcite and cleavage fractures within feldspar. Grain-boundary fractures mainly occur between mineral grains in linear contact. Dehydration during the conversion of clay minerals causes the formation of diagenetic shrinkage fractures (Fig. 4i). Core observations show that bedding fractures are most developed in mudstone, followed by dolomite, limestone, and siltstone, and are most poorly developed in the sandy conglomerate, coarse
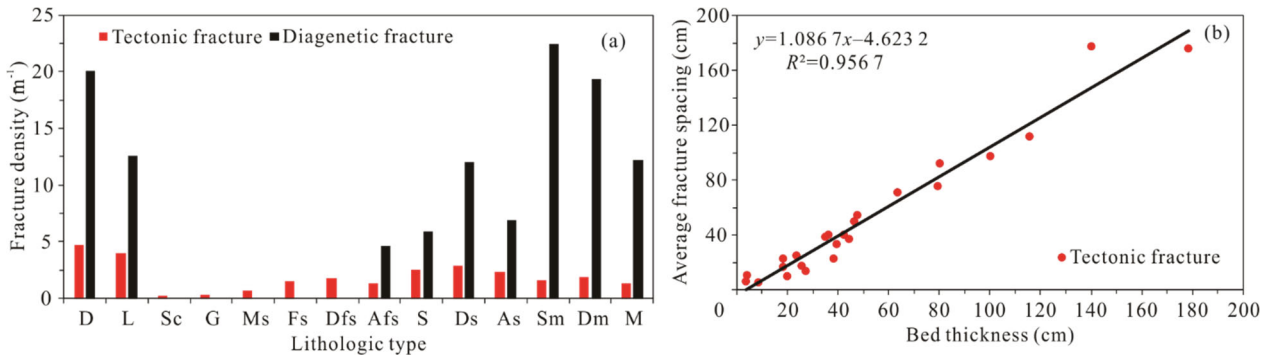
Figure 5. (a) Density distribution chart of fracture with different lithologic types; (b) relationship between fracture distance and bed thickness. D. Dolomite; L. limestone; Sc. sandy conglomerate; G. gritstone; Ms. medium sandstone; Fs. fine sandstone; Dfs. dolomitic fine sandstone; Afs. argillaceous fine sandstone; S. siltstone; Ds. dolomitic siltstone; As. argillaceous siltstone; Sm. silty mudstone; Dm. dolomitic mudstone; M. mudstone.
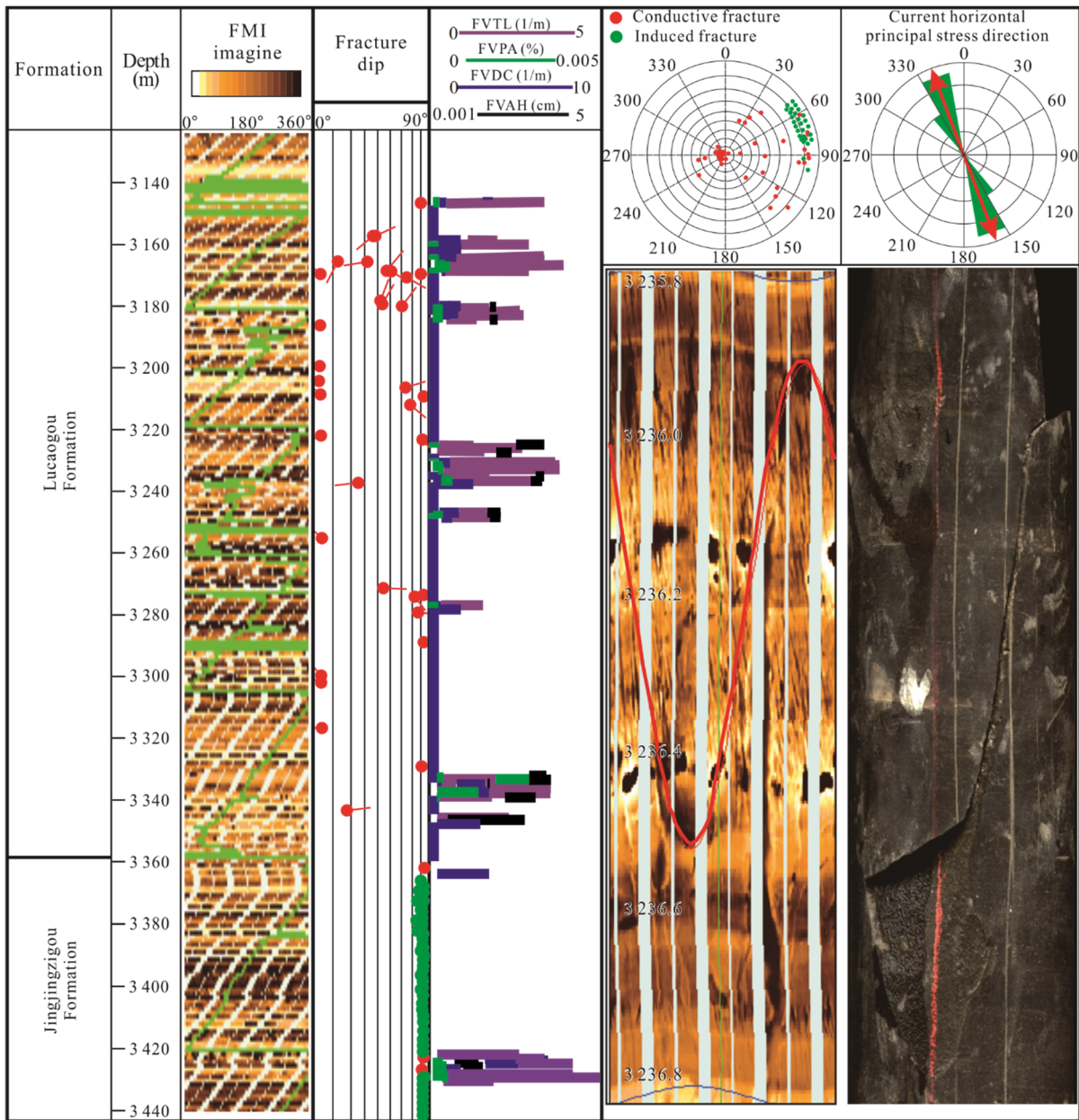

Figure 6. Interpretation result diagram of Well J8 FMI shows that the strike of maximum horizontal principal stress of Lucaogou Formation is the same as the strike of induced fractures of Jingjingzigou Formation.
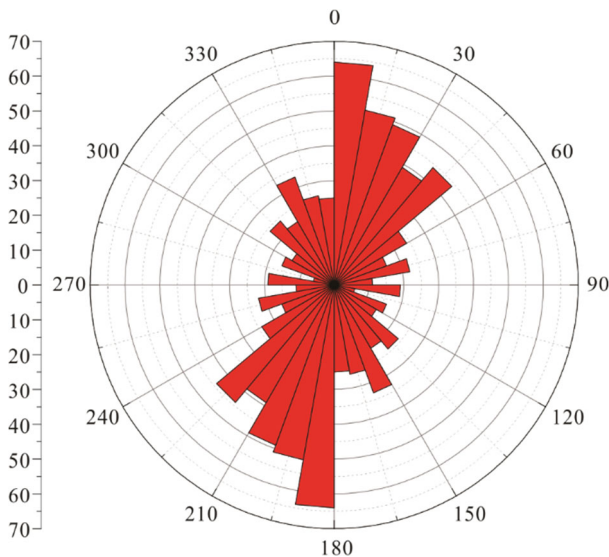
Figure 7. Rose diagram of the fracture strikes. The data from outcrop and FMI (*N*=542).

sandstone, medium sandstone, and fine sandstone (Fig 5a).

3.1.3 Overpressure-related fractures

The overpressure-related fractures are caused by overpressure fluid (Zeng, 2010). The origin of this kind of fracture is the hydraulic action with abnormally high fluid overpressure during formation (Liu et al., 2017). Under such abnormal fluid pressure, tensile stress can contribute to extensional fractures with different degrees of migration pathways and fracture apertures. They are generally irregular in shape, have inconsistent directions, limited extension, and random distribution. Some of them are characterized by grouped fracture veins, irregular dips, and various fracture apertures (Figs. 3g and 4e). They are filled with veins of calcite minerals after their formation, which restricts their effectiveness as oil charging and migration pathways.

Generally speaking, the tectonic fractures in tight sandstone reservoirs are mainly high-angle and vertical fractures, which tend to have an extensive extension range and are mostly filled with calcite. Tectonic fractures often appear in groups with obvious alignment and regularity, and the scale and complexity of fractures are affected by the structural stress properties, stress strength, and tectonic stages. Diagenetic fractures and overpressure-related fractures have nothing to do with tectonic movement or tectonic stress. They are generally irregular in shape, inconsistent in direction, limited in extension, and random in distribution. They are often controlled by diagenesis and overpressure.

3.2 Effectiveness of Natural Fractures

In underground reservoirs, natural fractures that are in an open state and can provide effective fluid flow channels are deemed to be effective fractures (Zeng et al., 2012). It has been pointed out in previous studies that the effectiveness of natural fractures is reflected by their filling and aperture features.

3.2.1 Filling characteristics

Based on their filling, fractures can be divided into three types: unfilled, partially filled, and fully filled fractures (Fig. 8a).

The unfilled and partially filled fractures possess nothing or some diagenetic material filling, and they are potentially open conduits for fluid flow. The filling states of the tectonic fractures, diagenetic fractures, and overpressure-related fractures are different, and their filling materials are mainly calcite (Figs. 3b and 3g), however, sometimes they are filled by carbonaceous clay (Fig. 3e). Fully filled tectonic fractures account for 8.69% of all fractures, and partially filled and unfilled fractures account for 32.50%. Among the diagenetic fractures, the fully filled fractures account for 1.04%, and partially filled and unfilled diagenetic fractures together account for 49.89% of all fractures. The overpressure-related fractures are all fully filled with calcite and account for 7.87% of all fractures. The statistical results preliminarily reflect that the degree of filling of the tectonic shear fractures is less than that of the bedding and overpressure-related fractures, indicating that shear fractures play a significant role in the seepage capacity of the tight oil reservoirs in the study area.

3.2.2 Fracture apertures and lengths

The length of a microfracture is from 0.78 to 197 µm (Fig. 8d). The actual aperture of a microfracture is between 0.1 and 50 µm (Fig. 8f). A tectonic microfracture has an aperture of 0.6–50 µm and a length of 8.1–158 µm. The aperture of a diagenetic fracture varies from 0.6 to 5 µm and its length ranges from 1.94 to 148 µm. The average aperture value of an overpressure-related fracture is <5 µm and its length varies from 0.78 to 197 µm. According to the FMI statistics of underground fracture apertures in the study area (Fig. 8e), the apertures of underground fractures in this area are all l <200 µm, with a peak value of less than 100 µm. The aperture value of each section is consistent with that of the underground fractures in FMIs.

3.3 Fracture Contributions to Physical Properties of Reservoir

We calculated the porosity and permeability of macroscopic fractures using image logging. Based on the Monte Carlo method, the porosity and permeability of the microfractures were evaluated using the corrected aperture value (Table 2). The average porosity of a tectonic fracture is 0.11%–0.22%, and its average permeability is from 13.20 to 53.10 mD. The average porosity and permeability of the tectonic microfractures are approximately 0.67% and 1.56 mD, respectively. The average porosity of the diagenetic fractures is approximately 0.06%, and its average permeability is approximately 6.02 mD, while the average porosity and permeability of the diagenetic microfractures are approximately 0.49% and 1.31 mD, respectively. The porosity and permeability of overpressure-related fractures are difficult to calculate. The overpressure-related fractures are the least abundant and exhibit poor effectiveness as oil reserves. Therefore, these fractures barely improve the tight reservoir porosity and permeability.

4 DISCUSSION
4.1 Factors Controlling the Effectiveness of Fractures

In the Lucaogou Formation, the present maximum principal stress is NNW trending (Fig. 6). The aperture of a tectonic fracture is affected by the direction of the maximum principal stress of the current geo-stress field (Fig. 9). However, fractures perpendicular to the current maximum principal stress have poor

effectiveness because the direction of the stress is perpendicular to the surface of fractures (Zeng and Li, 2009). In the study area,

fractures in the NNW direction have the largest apertures, followed by fractures in the N-S direction. Thus, seepage mainly
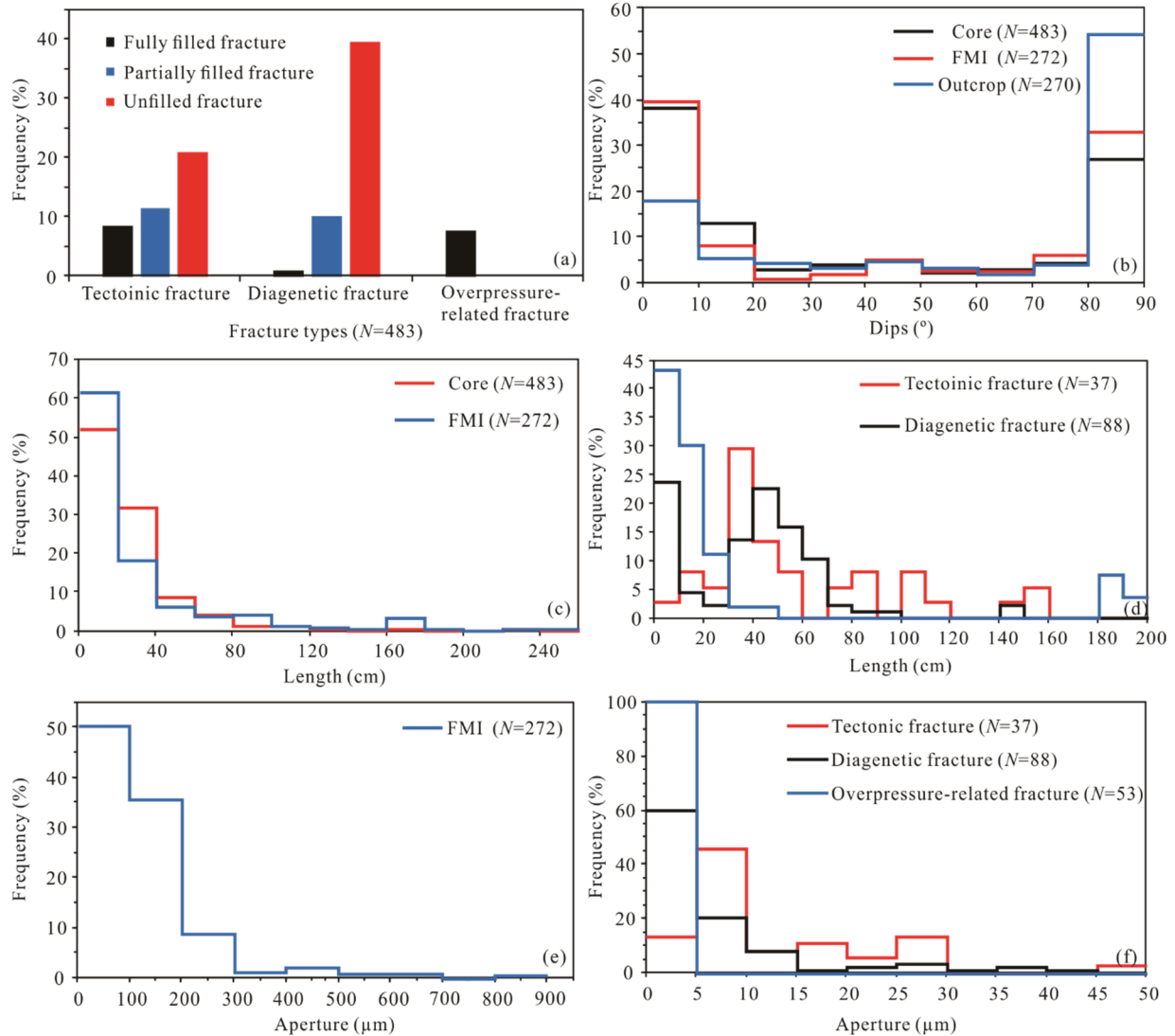

Figure 8. Statistical chart of different natural fracture parameters. (a) Distribution frequency diagram of filling property of natural fracture from the core observation; (b) distribution frequency diagram of inclination of natural fracture; (c) distribution frequency diagram of extension length of fractures; (d) distribution frequency of the length value of microfractures in the reservoir; the length value of tectonic microfractures, diagenetic microfractures, and overpressure-related fractures acquired by thin cast thin section and SEM; (e) distribution frequency diagram of nature fracture aperture in FMI; (f) distribution frequency of the aperture value of microfractures in the reservoir; the aperture value of tectonic microfractures, diagenetic microfractures, and overpressure-related fractures acquired by thin cast thin section and SEM.

Table 2 The fracture aperture, porosity, and permeability of different fractures

Fracture types	Tectonic fracture					Diagenetic fracture		Overpressure-related fracture[a]	
	Macro				Micro	Macro	Micro	Macro	Micro
Fracture strikes	N-S	NNE	NNW	NE	/	/	/	/	/
The mean fracture aperture (μm)	93.33	58.73	182.07	28.07	<10	<15	<10	/	/
The mean fracture length (μm)	5.43×10^5	3.44×10^5	3.60×10^5	3.02×10^5	68.89	0.69×10^5	39.56	4.48×10^4	<5
The mean fracture porosity (%)	0.13	0.16	0.22	0.11	0.67	0.06	0.49	/	/
The mean fracture permeability (mD)	29.9	17.84	53.1	13.2	1.56	6.02	1.31	/	/

Note: [a]. This kind of fracture is usually full-filled in the core or cast thin sections. Thus, it is too difficult to calculate porosity and permeability. The "/" means there is no data for that.
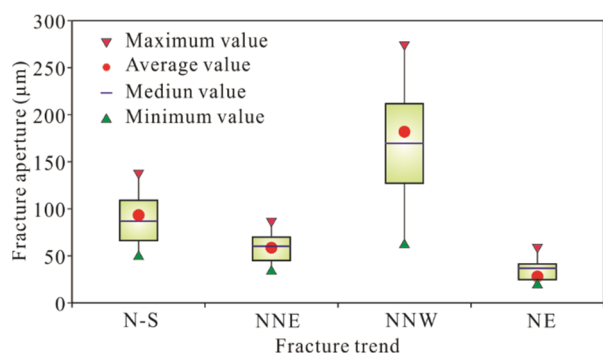
Figure 9. Box chart of the relationship between fracture trend and fracture aperture, data from FMI. The present maximum principal stress is NNW trending. N-S, *N*=69; NNE, *N*=22; NNW, *N*=43; NE, *N*=27.

occurs in NNW directions. When a fracture is parallel to the current maximum principal stress, the fracture achieves a large aperture, good connectivity, and high permeability; hence, this orientation of fractures can be regarded as the main seepage direction. The proportion of unfilled fractures and partially filled fractures is greater than 82% (Fig. 8a). Mineral particles existing in the partially filled fractures can play a supporting role to ensure that fractures remain open (Gong et al., 2015). Therefore, partially filled fractures are also effective fractures, indicating that, overall, all the observed fractures are relatively effective. These tight reservoirs have undergone multiple stages of diagenesis. For instance, in a period when a large amount of hydrocarbon was generated from the source rock, acidic fluid dissolved the fractures, shaping dissolution holes. Strong dissolution in a later stage improved the effectiveness of these fractures. On the other hand, fractures often close passages because of cementation or by being fully filled and solidified by fluids. Fractures formed in later stages are less likely to be filled; thus, it is easier for them to become effective fractures and to make a greater contribution to tight oil reservoirs. In the Middle and Late Cretaceous, many factors (like under-compaction, tectonic stress, and hydrocarbon-generating overpressure) led to overpressure (Zhang et al., 2019), of which the formation pressure coefficient always fluctuated between 1.00 and 1.6 (average 1.37) (Lian et al., 2016). The overpressure-related fractures are fully filled by calcite, and only a few such fractures can be opened by additional tectonic uplift (Fig. 4c). This kind of fracture has low permeability and thus makes a limited contribution to a tight oil reservoir. The angle of a fracture affects its effectiveness. The underground aperture and permeability of both low-angle tectonic fractures and horizontal diagenetic fractures are subject to the pressure from overlying strata. Therefore, these fractures are less effective than high-angle tectonic fractures in terms of migration. However, in the study area, horizontal and low-angle fractures are widely distributed with high density. Moreover, as their horizontal permeability is high, they might interweave among high-angle tectonic fractures (Fig. 3e), forming a fracture network system with relatively high permeability. This can result in good fracture connectivity, thus increasing the effectiveness of fractures.

4.2 Influence of Effective Fractures on Tight Oil

Effective fractures can affect the charging and accumulation of tight oil, and fractures with different types and apertures have distinct effects on accumulation of tight oil and reservoir formation. Generally, the fracture aperture is much larger than the critical pore throat radius (0.2 µm) (Pang et al., 2019). Under this condition, the migration and accumulation force of tight oil can change, making buoyancy the main reservoir-forming force. Subsequently, effective fractures become the preferential passages for tight oil and cause large scale accumulation at sweet spots. Existing intragranular fractures, grain-boundary fractures, and other nano-sized fractures, can be viewed as having larger pore throats if their apertures are equal to or less than the critical radius of a pore throat. In this condition, the greatest migration and accumulation force of buoyancy is approximately 0.088 MPa and the capillary pressure in the reservoir is approximately 0.11 MPa (Qiu et al., 2016a). Abnormally high pressure caused by hydrocarbon generation in source rock provides migration potential to tight oil (Li and Li, 2010). The pressure caused by hydrocarbon generation is much higher than the migration resistance of the tight oil in the Lucaogou Formation and is the main driving force for accumulation of tight oil (Qiu et al., 2016a). Unfilled high-angle tectonic fractures mostly play a role in the accumulation and charging of tight oil. In contrast, large-scale horizontal diagenetic fractures have a significant effect on the horizontal migration of tight oil.

Mudstones of the Lucaogou Formation have good potential for generating hydrocarbons, as do some siltstones (Cao et al., 2017). Tectonic fractures mainly exist in siltstone reservoirs, while diagenetic fractures, especially bedding fractures, develop in mudstones (source rocks) with a high density. The multicyclic evolution of the Jimsar sag resulted in multiple sets of source rocks and reservoir-cap rock assemblages. The primary source rocks in the sag were formed by rift-faulting in the extensional and transitional period after the Permian collision (Fang et al., 2006). Since the beginning of the Late Permian, mudstones and siltstones in the Lucaogou Formation have continued to generate hydrocarbons. The *R*o of the source rock maturity within tight oil reservoirs increases in the sequence of the matrix (average *R*o of 0.37%), and stylolite and bedding fracture (average *R*o of 0.72%), tectonic fracture (approximately average *R*o>2.38%) (Jiao et al., 2007). Organic matter preferentially converged in the pores of the rock matrix, before the formation of diagenetic and tectonic fractures. Thus, horizontal homogeneity is far stronger than vertical homogeneity. Under the formation load, hydrocarbon-bearing fluid caused diagenetic fractures (bedding fractures and stylolite) to move horizontally within the mudstone in the reservoir. These became the main channels for the primary horizontal migration of hydrocarbons. Some studies have confirmed that the mud source rocks and carbonate rocks preferentially drove hydrocarbon migration in the horizontal direction (Jiao et al., 2005; Leythaeuser et al., 1995). After tectonic fractures formed, when the hydrocarbon-bearing fluid moving in the horizontal direction encountered them, these fractures became the main migration channels and the hydrocarbon began to run vertically.

The carbon and oxygen isotope analysis of the tectonic fracture fillings indicates that the time of formation of fractures involved three stages (Fig. 10). The δ^{18}O of most of the samples is negative (δ^{18}O: -12.63‰ to -5.65‰) with fairly positive δ^{13}C values (δ^{13}C: -0.87‰ to 7.98‰) (Table 3). The average burial depth of the first fracture filling is 1 325 m, caused by the Indo-
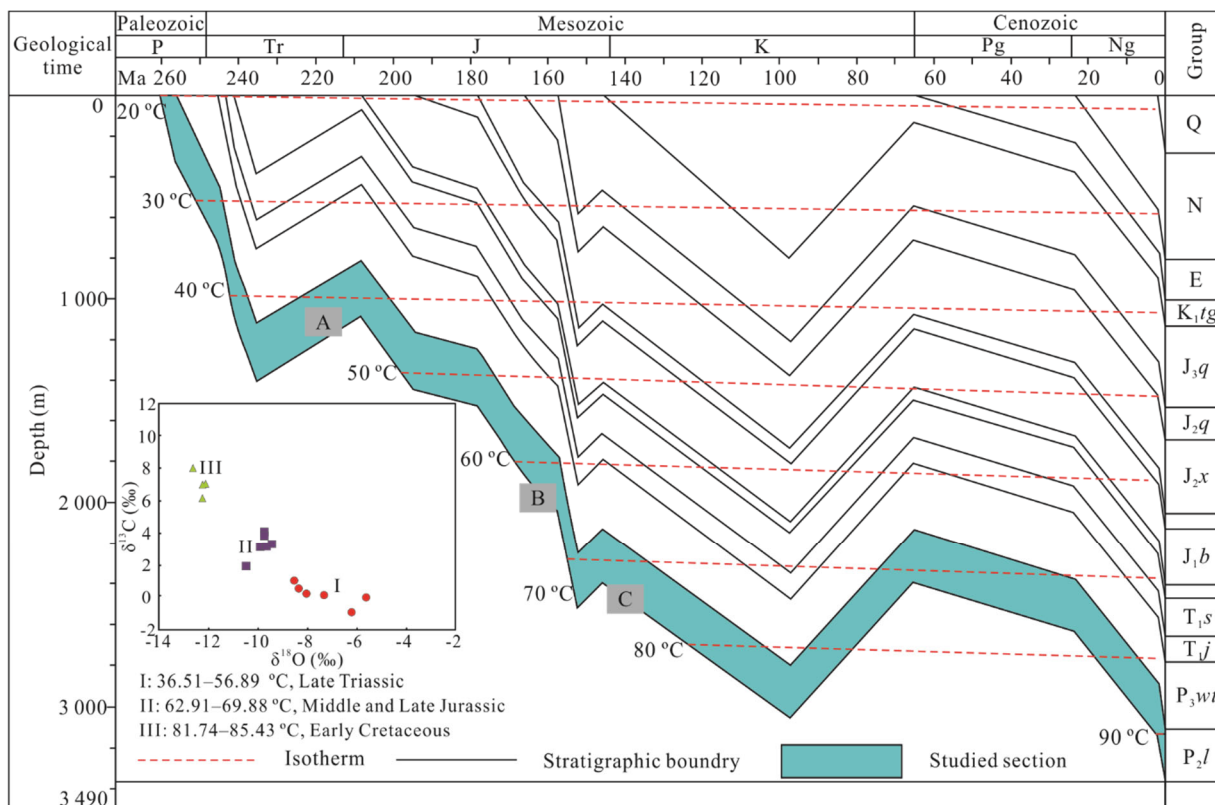
Figure 10. Geothermal history, burial history, and the temperature of veins in the tectonic fracture in the tight sandstone reservoir in the Permian Lucaogou Formation. The strata geothermal history and burial history are modified according to Wu et al. (2016, 2015). The data of the geothermal gradient are from Xi et al. (2015a), Yuan et al. (2015). The test data of carbon and oxygen isotope of calcite in tectonic fractures are from Zhang et al. (2017). A. The formation time of the tectonic fractures in the first stage; the temperature of carbon and oxygen isotope of calcite is between 36.51 and 56.89 ℃; B. the forming time of tectonic fractures in the second stage; the temperature of carbon and oxygen isotope of calcite is between 62.91 and 69.88 ℃; C. the forming time of tectonic fractures in the third stage; the temperature of carbon and oxygen isotope of calcite is between 81.74 and 85.438 ℃. P. Permian; Tr. Triassic; J. Jurassic; K. Cretaceous; Pg. Paleogene; Ng. Neogene.

Table 3   Carbon and oxygen isotopic composition of calcite fracture fills, data from Zhang et al. (2017)

| No.	Buried depth (m)	Lithology	Testing position	$\delta^{13}C$ (‰, PDB)	$\delta^{18}O$ (‰, PDB)	Formation temperature (℃)
1	4 056	Silt	Calcite vein	0.024	-5.648	39.509
2	4 122	Finestone	Calcite vein	4.02	-9.716	64.617
3	3 571.9	Silt	Calcite vein	0.159	-7.342	49.404
4	3 727.5	Muddy limestone	Calcite vein	3.896	-9.740	64.775
5	3 742	Silt	Calcite vein	6.98	-12.232	82.461
6	3 144	Silt	Calcite vein	0.562	-8.358	55.716
7	3 157.3	Silt	Calcite vein	6.146	-12.246	82.561
8	3 230.1	Muddy limestone	Calcite vein	3.139	-9.666	64.275
9	3 284	Silt	Calcite vein	7.045	-12.136	81.743
10	3 305	Limestone	Calcite vein	3.266	-9.462	62.912
11	3 637.2	Silt	Calcite vein	-0.865	-6.226	42.793
12	3 728	Limestone	Calcite vein	3.155	-9.922	66.007
13	3 755.2	Dolomite	Calcite vein	7.98	-12.635	85.479
14	3 789	Silt	Calcite vein	0.265	-8.053	53.794
15	2 281.6	Limestone	Calcite vein	1.956	-10.486	69.885
16	2 325	Medium sand	Calcite vein	1.056	-8.543	56.898
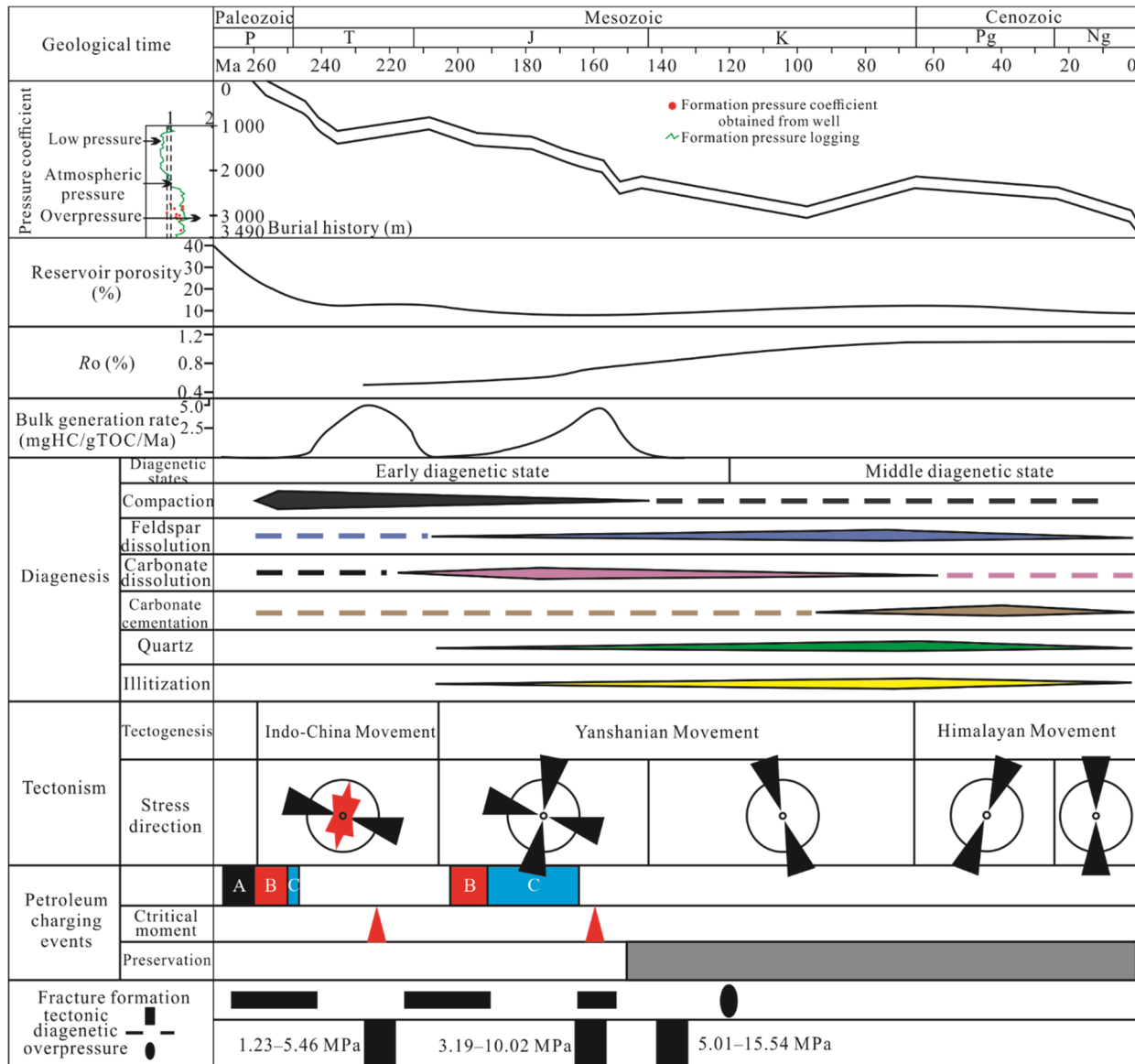
Figure 11. Diagram for petroleum system event and fracture formation time of the Permian Lucaogou Formation. Data related to burial history were obtained from Wu et al. (2015); data of pore evolution and diagenesis of the reservoir were from Wu et al. (2016); data of *R*o, efficiency of hydrocarbon expulsion, and petroleum system event were from Cao et al. (2017), Qiu et al. (2016c); data of tectonic action were from Kang et al. (2011); efficiency of formation pressure was from Lian et al. (2016), Li et al. (2010). A. Source rock; B. reservoir; C. caprock; P. Permian; T. Triassic; J. Jurassic; K. Cretaceous; Pg. Paleogene; Ng. Neogene.

China Movement in the Late Triassic. The second stage has an average burial depth of 2 095 m, and the fracture formation period was in the Middle and Late Jurassic. The third stage formed at an average burial depth of 2 845 m in the Early Cretaceous. The homogenization temperatures of fluid inclusions from wells J174 and J176 were 75 to 95 ℃ and 105 to 115 ℃, respectively (Cao et al., 2017). This shows the different temperatures at which the two oil charging events occurred in the Lucaogou Formation. Tight oil generation and charging mainly occurred in the Triassic (235–210 Ma) and Jurassic (180–150 Ma), and the tectonic fractures in the formation formed in three stages. The time of oil charging matched the formation time of the first and second tectonic fractures. The fractures in the first stage formed in the Late Triassic, which coincided with the charging time of the tight oil in the first stage. This happened before the porosity and permeability of the matrix decreased significantly when the porosity

and permeability of the matrix in the tight oil reservoir were much lower than those of the fractures. The development of tectonic fractures formed a low-pressure zone (Jiang et al., 2015), lowering the initial charging threshold of oil and helping the tight oil to migrate preferentially into the fractures of the tight sandstone reservoir. The formation of tectonic fractures in the first stage significantly improved the permeability of the reservoir and provided oil seepage channels for the tight sandstone reservoir. The second stage tectonic fractures formed in the Middle and Late Jurassic, coinciding with the charging time of oil in the second stage; however, this happened after the porosity of the matrix had decreased significantly (porosity <10%) (Fig. 11). At this stage, the tectonic fractures not only improved previously poor porosity and permeability but also formed the main seepage passages and became important reservoir spaces of tight oil. The tectonic fracture in the third stage formed in the Early Cretaceous,

when oil charging stopped. However, the formation time of the fractures in this stage coincided with the oil preservation time (Fig. 11). Tectonic fractures in this stage served as migration channels of oil and readjusted the accumulation and distribution of oil in the Lucaogou Formation. This probably caused some damages to the preservation of tight oil.

4.3 Influence of Fractures on Tight Oil Productivity

The overall low permeability of the matrix pores is the main reason for the low productivity of tight oil formations. The calculated permeabilities of the natural fractures are several orders of magnitude greater than those of the matrix pores (0.1 mD), which indicates that the fracture improved the permeability of the tight sandstones. Combining with the production data of Well J8, the results from analysis of fracture parameter analysis show that different types of natural fractures had different effects on the average daily production of tight oil. The wells within the area in which tectonic fractures are well developed are typically associated with the highest oil yield (Fig. 12). The fracture permeability is scale-related (Guerriero et al., 2013), where tectonic fractures are related to the largest scale (Table 2). At the same scale, multiple factors, including the fracture shape, aperture, cementation, and dissolution can influence fracture permeability (Bisdom et al., 2016; Lander and Laubach, 2015; Laubach et al., 2004). High angle tectonic shear fractures without mineral filling are mainly developed in the oil test zone, in which no dissolution could be found. Owing to the high dip angle, the fracture

aperture is less affected by the pressure of the overlying strata. The aperture of tectonic fractures can determine the permeability of these fractures without mineral filling, i.e., the aperture determines the flow capacity of underground fluids. Wells with well-developed bedding are featured with lower vertical permeability, higher horizontal permeability, and lower daily oil test yield. Bedding fractures improve the horizontal permeability of the tight oil reservoirs. When the bedding fractures are well developed, their horizontal permeability is enhanced to a certain degree (Fig. 12). As the bedding fractures are distributed discontinuously with transverse connectivity, under an overlying confining pressure, they are commonly close, and have small apertures and low permeability. The wells with well-developed overpressure-related fractures have the lowest oil test yield (Fig. 12), because these fractures are fully filled with calcite and have the smallest fracture size, leading to exceedingly low porosity and permeability. In this section, the vertical and horizontal permeability is the lowest, and the oil test yield is also the lowest. Therefore, tectonic fractures with high dip angles control the flow system of the tight reservoirs, and they should be used as the primary basis for understanding the patterns of tight oil accumulation.

In Well J16, the average daily oil test capacity in sections A, B, C, and D is <1, 1–5, 5–10, and >10 t/day, respectively (Fig. 13). Tectonic fractures were not observed in the core and imaging logging data from Section B, which had the lowest production capacity as its weak porosity was solely provided by the matrix.
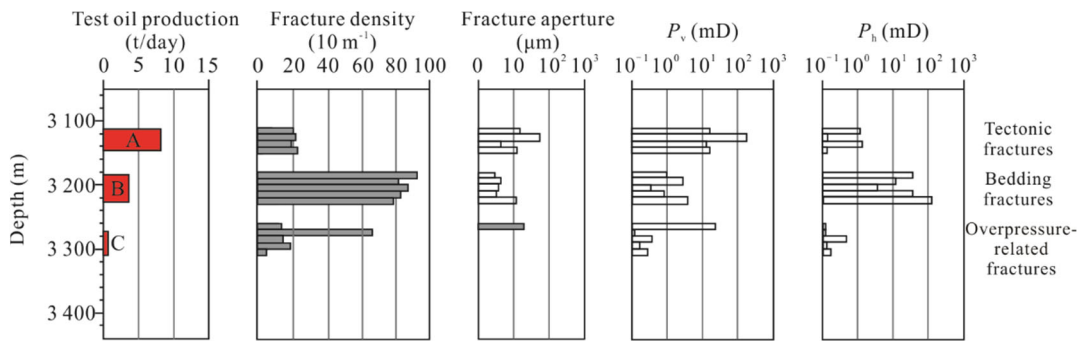

Figure 12. The relationship between test oil production and natural fracture types in Well J8. P_v. Vertical permeability; P_h. horizontal permeability.
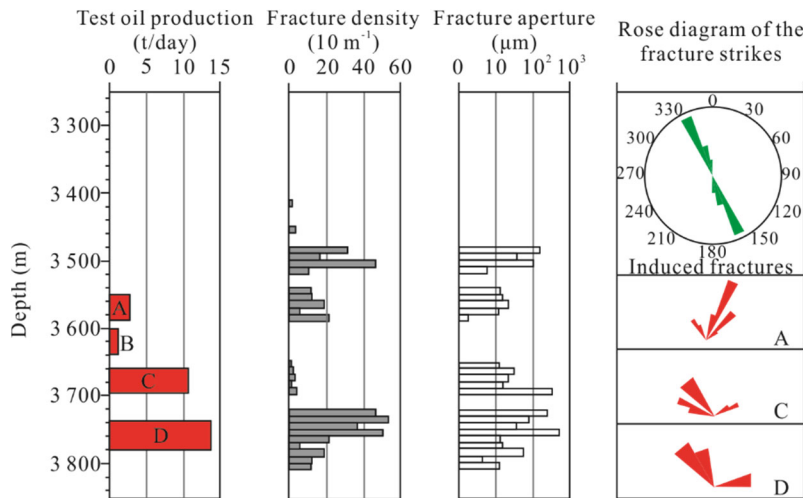

Figure 13. The relationship between test oil production and natural fracture attributes in Well J16.
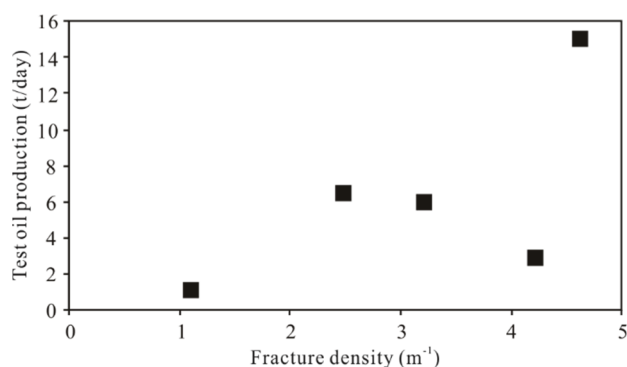
Figure 14. The relationship between fracture density and test oil production.

Tectonic fractures are mainly developed in sections A, C, and D; however, the corresponding relationship between fracture density and productivity seems unclear. There is a weak positive correlation between the daily production of oil and fracture density of the 5 test wells (Fig. 14). Combined with a previous analysis of the production data of 189 horizontal wells and 24 vertical wells in the Ordos Basin (Lyu et al., 2019), the initial oil production of vertical wells presents a positive correlation with fracture abundance. It could be inferred that the density of a natural fracture has a positive effect on the production of tight oil. Compared with the effect of the density of natural fractures on tight oil production, it is believed that aperture of a natural fracture is closely related to tight oil production capacity. The aperture of tectonic fractures is less affected by diagenesis and more affected by the current direction of maximum principal stress. In the oil test zone, higher proportions of fractures parallel to the current maximum principal stress direction lead to larger fracture apertures and stronger seepage capacity, resulting in higher daily oil test yield.

5 CONCLUSIONS

(1) Three types of natural fractures developed in the Permian Lucaogou Formation, namely, tectonic fractures, diagenetic fractures, and overpressure-related fractures, respectively. There are various kinds of diagenetic fractures, including bedding fractures, stylolites, intragranular fractures, grain-boundary fractures, and diagenetic shrinkage fractures. Macrofractures are major migration channels, and microfractures could be viewed as larger pore throats that serve as storage space.

(2) The lithology determines the density of the fractures, and the bed thickness constraints the length of the fractures. Tectonic fractures mainly develop in sandstone and dolomite. The grain size and brittle content in the same lithology determine the extent of tectonic fractures. The intensity decreases with an increase in bed thickness (R^2=0.956 7). Bedding fractures best develop in mudstone, followed by dolomite, limestone, and siltstone. They are poorly developed in sandy conglomerate, coarse sandstone, medium sandstone, and fine sandstone.

(3) Tectonic fractures in the study area formed in three stages: Late Triassic, Middle–Late Jurassic, and Early Cretaceous. Diagenetic fractures formed along with the diagenesis, before the formation of the tectonic fractures, while the overpressure-related fractures formed mainly during the Middle and Late Jurassic.

(4) The bedding fractures and the stylolites function as the primary migration channels. The intergranular, grain-boundary, and diagenetic shrinkage fractures share continuity along micropores to increase the connectivity of tight sandstone. Meanwhile, the first and second tectonic fracture stages ensured the effective charging of tight oil, and the third phase of tectonic fractures readjusted the accumulation and distribution of tight oil in the formation. The overpressure-related fractures are fully filled with calcite and thus make limited contributions to the effectiveness of the tight reservoir.

(5) Natural fractures are the critical factor influencing tight oil production. The tectonic fractures with high dip angles control the flow system of the tight reservoirs, and they should be used as the main basis for understanding the pattern of oil accumulation. The current principal stress effectively controls the fracture apertures, which determines the effectiveness of fractures; hence, its direction is the critical factor influencing the effectiveness of fractures.

REFERENCES CITED

Al-Aasm, I. S., Coniglio, M., Desrochers, A., 1995. Formation of Complex Fibrous Calcite Veins in Upper Triassic Strata of Wrangellia Terrain, British Columbia, Canada. *Sedimentary Geology*, 100(1/2/3/4): 83–95. https://doi.org/10.1016/0037-0738(95)00104-2

Ameen, M. S., Hailwood, E. A., 2008. A New Technology for the Characterization of Microfractured Reservoirs (Test Case: Unayzah Reservoir, Wudayhi Field, Saudi Arabia). *AAPG Bulletin*, 92(1): 31–52. https://doi.org/10.1306/08200706090

Anders, M. H., Laubach, S. E., Scholz, C. H., 2014. Microfractures: A Review. *Journal of Structural Geology*, 69: 377–394. https://doi.org/10.1016/j.jsg.2014.05.011

Bai, H., Pang, X. Q., Kuang, L. C., et al., 2017. Hydrocarbon Expulsion Potential of Source Rocks and Its Influence on the Distribution of Lacustrine Tight Oil Reservoir, Middle Permian Lucaogou Formation, Jimsar Sag, Junggar Basin, Northwest China. *Journal of Petroleum Science and Engineering*, 149: 740–755. https://doi.org/10.1016/j.petrol.2016.09.053

Becker, S. P., Eichhubl, P., Laubach, S. E., et al., 2010. A 48 M.y. History of Fracture Opening, Temperature, and Fluid Pressure: Cretaceous Travis Peak Formation, East Texas Basin. *Geological Society of America Bulletin*, 122(7/8): 1081–1093. https://doi.org/10.1130/b30067.1

Bisdom, K., Bertotti, G., Nick, H. M., 2016. The Impact of *in-situ* Stress and Outcrop-Based Fracture Geometry on Hydraulic Aperture and Upscaled Permeability in Fractured Reservoirs. *Tectonophysics*, 690: 63–75. https://doi.org/10.1016/j.tecto.2016.04.006

Bruna, P. O., Lavenu, A. P. C., Matonti, C., et al., 2019. Are Stylolites Fluid-Flow Efficient Features?. *Journal of Structural Geology*, 125: 270–277. https://doi.org/10.1016/j.jsg.2018.05.018

Caja, M. A., Permanyer, A., Marfil, R., et al., 2006. Fluid Flow Record from Fracture-Fill Calcite in the Eocene Limestones from the South-Pyrenean Basin (NE Spain) and Its Relationship to Oil Shows. *Journal of Geochemical Exploration*, 89(1/2/3): 27–32. https://doi.org/10.1016/j.gexplo.2005.11.009

Cao, Z., Liu, G. D., Xiang, B. L., et al., 2017. Geochemical Characteristics of Crude Oil from a Tight Oil Reservoir in the Lucaogou Formation, Jimusar Sag, Junggar Basin. *AAPG Bulletin*, 101(1): 39–72. https://doi.org/10.1306/05241614182

Evans, M. A., Battles, D. A., 1999. Fluid Inclusion and Stable Isotope Analyses of Veins from the Central Appalachian Valley and Ridge Province: Implications for Regional Synorogenic Hydrologic Structure and Fluid Migration. *Geological Society of America Bulletin*, 111(12): 1841–1860. https://doi.org/10.1130/0016-7606(1999)1111841:fiasia>2.3.co;2

Fall, A., Eichhubl, P., Cumella, S. P., et al., 2012. Testing the Basin-Centered Gas Accumulation Model Using Fluid Inclusion Observations: Southern Piceance Basin, Colorado. *AAPG Bulletin*, 96(12): 2297–2318. https://doi.org/10.1306/05171211149

Fang, S. H., Jia, C. Z., Guo, Z. J., et al., 2006. New View on the Permian Evolution of the Junggar Basin and Its Implications for Tectonic Evolution. *Earth Science Frontiers*, 13(3): 108–121 (in Chinese with English Abstract)

Fang, S. H., Song, Y., Xu, H. M., 2007. Relationship between Tectonic Evolution and Petroleum System Formation—Taking the Jimsar Sag of Eastern Junggar Basin as an Example. *Petroleum Geology & Experiment*, 29(2): 149–153, 161 (in Chinese with English Abstract)

Ghosh, S., Galvis-Portilla, H. A., Klockow, C. M., et al., 2018. An Application of Outcrop Analogues to Understanding the Origin and Abundance of Natural Fractures in the Woodford Shale. *Journal of Petroleum Science and Engineering*, 164: 623–639. https://doi.org/10.1016/j.petrol.2017.11.073

Giletti, B. J., 1986. Diffusion Effects on Oxygen Isotope Temperatures of Slowly Cooled Igneous and Metamorphic Rocks. *Earth and Planetary Science Letters*, 77(2): 218–228. https://doi.org/10.1016/0012-821x(86)90162-7

Gong, L., Gao, M. Z., Zeng, L. B., et al., 2017. Controlling Factors on Fracture Development in the Tight Sandstone Reservoirs: A Case Study of Jurassic-Neogene in the Kuqa Foreland Basin. *Natural Gas Geoscience*, 28(2): 199–208. https://doi.org/10.11764/j.issn.1672-1926.2016.12.003 (in Chinese with English Abstract)

Gong, L., Zeng, L. B., Du, Y., et al., 2015. Influences of Structural Diagenesis on Fracture Effectiveness: A Case Study of the Cretaceous Tight Sandstone Reservoirs of Kuqa Foreland Basin. *Journal of China University of Mining & Technology*, 44(3): 514–519. https://doi.org/10.13247/j.cnki.jcumt.000263 (in Chinese with English Abstract)

Gross, M. R., Eyal, Y., 2007. Throughgoing Fractures in Layered Carbonate Rocks. *Geological Society of America Bulletin*, 119(11/12): 1387–1404. https://doi.org/10.1130/0016-7606(2007)119[1387:tfilcr]2.0.co;2

Guerriero, V., Mazzoli, S., Iannace, A., et al., 2013. A Permeability Model for Naturally Fractured Carbonate Reservoirs. *Marine and Petroleum Geology*, 40: 115–134. https://doi.org/10.1016/j.marpetgeo.2012.11.002

Guo, Q. L., Wang, S. J., Chen, X. M., 2019. Assessment on Tight Oil Resources in Major Basins in China. *Journal of Asian Earth Sciences*, 178: 52–63. https://doi.org/10.1016/j.jseaes.2018.04.039

Han, Y. J., Horsfield, B., Wirth, R., et al., 2017. Oil Retention and Porosity Evolution in Organic-Rich Shales. *AAPG Bulletin*, 101(6): 807–827. https://doi.org/10.1306/09221616069

Hennings, P., 2009. AAPG-SPE-SEG Hedberg Research Conference on "the Geologic Occurrence and Hydraulic Significance of Fractures in Reservoirs". *AAPG Bulletin*, 93(11): 1407–1412. https://doi.org/10.1306/intro931109

Hennings, P. H., Olson, J. E., Thompson, L. B., 2000. Combining Outcrop Data and Three-Dimensional Structural Models to Characterize Fractured Reservoirs: An Example from Wyoming. *AAPG Bulletin*, 84(6): 830–849. https://doi.org/10.1306/a967340a-1738-11d7-8645000102c1865d

Howard, J. H., Nolen-Hoeksema, R. C., 1990. Description of Natural Fracture Systems for Quantitative Use in Petroleum Geology. *AAPG Bulletin*, 74(2): 151–162. https://doi.org/10.1306/0c9b2281-1710-11d7-8645000102c1865d

Jia, C. Z., Zou, C. N., Li, J. J., et al., 2012. Assessment Criteria, Main Types, Basic Features and Resource Prospects of the Tight Oil in China. *Acta Petrolei Sinica*, 33(3): 343–350. https://doi.org/10.1016/s2096-2495(17)30026-1 (in Chinese with English Abstract)

Jiang, Z. X., Li, F., Yang, H. J., et al., 2015. Development Characteristics of Fractures in Jurassic Tight Reservoir in Dibei Area of Kuqa Depression and Its Reservoir-Controlling Mode. *Acta Petrolei Sinica*, 36(S2): 102–111. https://doi.org/10.7623/Syxb2015s2009 (in Chinese with English Abstract)

Jiao, Y. Q., Wu, L. Q., He, M. C., et al., 2007. Occurrence, Thermal Evolution and Primary Migration Processes Derived from Studies of Organic Matter in the Lucaogou Source Rock at the Southern Margin of the Junggar Basin, NW China. *Science in China Series D: Earth Sciences*, 50(2): 114–123. https://doi.org/10.1007/s11430-007-6027-9

Jiao, Y. Q., Yan, J. X., Li, S. T., et al., 2005. Architectural Units and Heterogeneity of Channel Reservoirs in the Karamay Formation, Outcrop Area of Karamay Oil Field, Junggar Basin, Northwest China. *AAPG Bulletin*, 89(4): 529–545. https://doi.org/10.1306/10040400955

Ju, W., Sun, W. F., 2016. Tectonic Fractures in the Lower Cretaceous Xiagou Formation of Qingxi Oilfield, Jiuxi Basin, NW China Part One: Characteristics and Controlling Factors. *Journal of Petroleum Science and Engineering*, 146: 617–625. https://doi.org/10.1016/j.petrol.2016.07.042

Ju, W., Wang, J. L., Fang, H. H., et al., 2019. Paleotectonic Stress Field Modeling and Prediction of Natural Fractures in the Lower Silurian Longmaxi Shale Reservoirs, Nanchuan Region, South China. *Marine and Petroleum Geology*, 100: 20–30. https://doi.org/10.1016/j.marpetgeo.2018.10.052

Ju, W., Wu, C. F., Wang, K., et al., 2017. Prediction of Tectonic Fractures in Low Permeability Sandstone Reservoirs: A Case Study of the $E_{s_3}m$ Reservoir in the Block Shishen 100 and Adjacent Regions, Dongying Depression. *Journal of Petroleum Science and Engineering*, 156: 884–895. https://doi.org/10.1016/j.petrol.2017.06.068

Kang, Y. Z., Wang, Z., Kang, Z., 2011. Study on Oil Control of Structural System in Junggar-Tuha Basin. Geological Press, Beijing. 127–132 (in Chinese)

Khoshbakht, F., Azizzadeh, M., Memarian, H., et al., 2012. Comparison of Electrical Image Log with Core in a Fractured Carbonate Reservoir. *Journal of Petroleum Science and Engineering*, 86/87: 289–296. https://doi.org/10.1016/j.petrol.2012.03.007

Kuang, L. C., Hu, W. X., Wang, X. L., et al., 2013. Research of the Tight Oil Reservoir in the Lucaogou Formation in Jimusar Sag: Analysis of Lithology and Porosity Characteristics. *Geological Journal of China Universities*, 19(3): 529–535. https://doi.org/10.16108/j.issn1006-7493.2013.03.003 (in Chinese with English Abstract)

Kuang, L. C., Tang, Y., Lei, D. W., et al., 2012. Formation Conditions and Exploration Potential of Tight Oil in the Permian Saline Lacustrine

Dolomitic Rock, Junggar Basin, NW China. *Petroleum Exploration and Development*, 39(6): 700–711. https://doi.org/10.1016/s1876-3804(12)60095-0

Lai, J., Wang, G. W., Fan, Z. Y., et al., 2017. Three-Dimensional Quantitative Fracture Analysis of Tight Gas Sandstones Using Industrial Computed Tomography. *Scientific Reports*, 7(1): 1825. https://doi.org/10.1038/s41598-017-01996-7

Lai, J., Wang, G. W., Wang, S., et al., 2018. A Review on the Applications of Image Logs in Structural Analysis and Sedimentary Characterization. *Marine and Petroleum Geology*, 95: 139–166. https://doi.org/10.1016/j.marpetgeo.2018.04.020

Lander, R. H., Laubach, S. E., 2015. Insights into Rates of Fracture Growth and Sealing from a Model for Quartz Cementation in Fractured Sandstones. *Geological Society of America Bulletin*, 127(3/4): 516–538. https://doi.org/10.1130/b31092.1

Laubach, S. E., 2003. Practical Approaches to Identifying Sealed and Open Fractures. *AAPG Bulletin*, 87(4): 561–579. https://doi.org/10.1306/11060201106

Laubach, S. E., 1989. Paleostress Directions from the Preferred Orientation of Closed Microfractures (Fluid-Inclusion Planes) in Sandstone, East Texas Basin, USA. *Journal of Structural Geology*, 11(5): 603–611. https://doi.org/10.1016/0191-8141(89)90091-6

Laubach, S. E., 1988. Subsurface Fractures and Their Relationship to Stress History in East Texas Basin Sandstone. *Tectonophysics*, 156(1/2): 37–49. https://doi.org/10.1016/0040-1951(88)90281-8

Laubach, S. E., Eichhubl, P., Hilgers, C., et al., 2010. Structural Diagenesis. *Journal of Structural Geology*, 32(12): 1866–1872. https://doi.org/10.1016/j.jsg.2010.10.001

Laubach, S. E., Lander, R. H., Criscenti, L. J., et al., 2019. The Role of Chemistry in Fracture Pattern Development and Opportunities to Advance Interpretations of Geological Materials. *Reviews of Geophysics*, 57(3): 1065–1111. https://doi.org/10.1029/2019rg000671

Laubach, S. E., Olson, J. E., Gross, M. R., 2009. Mechanical and Fracture Stratigraphy. *AAPG Bulletin*, 93(11): 1413–1426. https://doi.org/10.1306/07270909094

Laubach, S. E., Olson, J. E., Gale, J. F. W., 2004. Are Open Fractures Necessarily Aligned with Maximum Horizontal Stress?. *Earth and Planetary Science Letters*, 222(1): 191–195. https://doi.org/10.1016/j.epsl.2004.02.019

Leythaeuser, D., Borromeo, O., Mosca, F., et al., 1995. Pressure Solution in Carbonate Source Rocks and Its Control on Petroleum Generation and Migration. *Marine and Petroleum Geology*, 12(7): 717–733. https://doi.org/10.1016/0264-8172(95)93597-w

Li, M. C., Li, J., 2010. "Dynamic Trap": A Main Action of Hydrocarbon Charging to Form Accumulations in Low Permeability-Tight Reservoir. *Acta Petrolei Sinica*, 31(5): 718–722 (in Chinese with English Abstract)

Li, P. L., Feng, J. H., Lu, Y. C., et al., 2010. Tectonic Sedimentation and Accumulation in the Junggar Basin. Geological Press, Beijing. 237–240 (in Chinese)

Lian, H., Zha, M., Gao, C. H., et al., 2016. Abnormal High Pressure and Tight Oil Enrichment of Lucaogou Formation in Jimusaer Sag. *Xinjiang Petroleum Geology*, 37(2): 163–168 (in Chinese with English Abstract)

Liu, C., Liu, K. Y., Wang, X. Q., et al., 2019. Chemo-Sedimentary Facies Analysis of Fine-Grained Sediment Formations: An Example from the Lucaogou Fm in the Jimusaer Sag, Junggar Basin, NW China. *Marine and Petroleum Geology*, 110: 388–402. https://doi.org/10.1016/j.marpetgeo.2019.06.043

Liu, D. D., Yang, D. X., Zhang, Z. Y., et al., 2019. Fracture Identification for Tight Reservoirs by Conventional and Imaging Logging: A Case Study of Permian Lucaogou Formation in Jimsar Sag, Junggar Basin. *Lithologic Reservoirs*, 31(3): 76–85 (in Chinese with English Abstract)

Liu, D. D., Zhang, C., Luo, Q., et al., 2017. Development Characteristics and Controlling Factors of Natural Fractures in Permian Lucaogou Formation Tight Reservoir in Jimsar Sag, Junggar Basin. *China Petroleum Exploration*, 22(4): 36–47 (in Chinese with English Abstract)

Liu, J. S., Ding, W. L., Yang, H. M., et al., 2018. Quantitative Prediction of Fractures Using the Finite Element Method: A Case Study of the Lower Silurian Longmaxi Formation in Northern Guizhou, South China. *Journal of Asian Earth Sciences*, 154: 397–418. https://doi.org/10.1016/j.jseaes.2017.12.038

Luo, X. R., Wang, Z. M., Zhang, L. Q., et al., 2007. Overpressure Generation and Evolution in a Compressional Tectonic Setting, the Southern Margin of Junggar Basin, Northwestern China. *AAPG Bulletin*, 91(8): 1123–1139. https://doi.org/10.1306/02260706035

Lyu, W. Y., Zeng, L. B., Zhang, B. J., et al., 2017. Influence of Natural Fractures on Gas Accumulation in the Upper Triassic Tight Gas Sandstones in the Northwestern Sichuan Basin, China. *Marine and Petroleum Geology*, 83: 60–72. https://doi.org/10.1016/j.marpetgeo.2017.03.004

Lyu, W. Y., Zeng, L. B., Zhou, S. B., et al., 2019. Natural Fractures in Tight-Oil Sandstones: A Case Study of the Upper Triassic Yanchang Formation in the Southwestern Ordos Basin, China. *AAPG Bulletin*, 103(10): 2343–2367. https://doi.org/10.1306/0130191608617115

Mahmoud, M., Hamza, A., Hussein, I. A., et al., 2020. Carbon Dioxide EGR and Sequestration in Mature and Immature Shale: Adsorption Study. *Journal of Petroleum Science and Engineering*, 188: 106923. https://doi.org/10.1016/j.petrol.2020.106923

McGlade, C. E., 2012. A Review of the Uncertainties in Estimates of Global Oil Resources. *Energy*, 47(1): 262–270. https://doi.org/10.1016/j.energy.2012.07.048

Nelson, P. H., 2009. Pore-Throat Sizes in Sandstones, Tight Sandstones, and Shales. *AAPG Bulletin*, 93(3): 329–340. https://doi.org/10.1306/10240808059

Olson, J. E., Laubach, S. E., Eichhubl, P., 2010. Estimating Natural Fracture Producibility in Tight Gas Sandstones: Coupling Diagenesis with Geomechanical Modeling. *The Leading Edge*, 29(12): 1494–1499. https://doi.org/10.1190/1.3525366

Olson, J. E., Laubach, S. E., Lander, R. H., 2009. Natural Fracture Characterization in Tight Gas Sandstones: Integrating Mechanics and Diagenesis. *AAPG Bulletin*, 93(11): 1535–1549. https://doi.org/10.1306/08110909100

Ozkan, A., Cumella, S. P., Milliken, K. L., et al., 2011. Prediction of Lithofacies and Reservoir Quality Using Well Logs, Late Cretaceous Williams Fork Formation, Mamm Creek Field, Piceance Basin, Colorado. *AAPG Bulletin*, 95(10): 1699–1723. https://doi.org/10.1306/01191109143

Pang, H., Ding, X. G., Pang, X. Q., et al., 2019. Lower Limits of Petrophysical Parameters Allowing Tight Oil Accumulation in the Lucaogou Formation, Jimusaer Depression, Junggar Basin, Western China. *Marine and Petroleum Geology*, 101: 428–439. https://doi.org/10.1016/j.marpetgeo.2018.12.021

Pang, Z. L., Zou, C. N., Tao, S. Z., et al., 2012. Formation, Distribution and Resource Evaluation of Tight Oil in China. *Engineering Sciences*, 14(7): 60–67 (in Chinese with English Abstract)

Perez, R. J., Boles, J. R., 2004. Mineralization, Fluid Flow, and Sealing Properties Associated with an Active Thrust Fault: San Joaquin Basin, California. *AAPG Bulletin*, 88(9): 1295–1314. https://doi.org/10.1306/03170403028

Prioul, R., Donald, A., Koepsell, R., et al., 2007. Forward Modeling of Fracture-Induced Sonic Anisotropy Using a Combination of Borehole Image and Sonic Logs. *Geophysics*, 72(4): E135–E147. https://doi.org/10.1190/1.2734546

Prioul, R., Jocker, J., 2009. Fracture Characterization at Multiple Scales Using Borehole Images, Sonic Logs, and Walkaround Vertical Seismic Profile. *AAPG Bulletin*, 93(11): 1503–1516. https://doi.org/10.1306/08250909019

Qiu, Z., Shi, Z. S., Dong, D. Z., et al., 2016a. Geological Characteristics of Source Rock and Reservoir of Tight Oil and Its Accumulation Mechanism: A Case Study of Permian Lucaogou Formation in Jimusar Sag, Junggar Basin. *Petroleum Exploration and Development*, 43(6): 1013–1024. https://doi.org/10.1016/s1876-3804(16)30118-5

Qiu, Z., Wu, X. Z., Tang, Y., et al., 2016b. Resource Assessment of Tight Oil from the Permian Lucaogou Formation in Jimusar Sag, Junggar Basin, China. *Natural Gas Geoscience*, 27(9): 1688–1698 (in Chinese with English Abstract)

Qiu, Z., Zou, C. N., Dong, D. Z., et al., 2016c. Petroleum System Assessment of Conventional-Unconventional Oil in the Jimusar Sag, Junggar Basin, Northwest China. *Journal of Unconventional Oil and Gas Resources*, 16: 53–61. https://doi.org/10.1016/j.juogr.2016.09.005 (in Chinese with English Abstract)

Santos, R. F. V. C., Miranda, T. S., Barbosa, J. A., et al., 2015. Characterization of Natural Fracture Systems: Analysis of Uncertainty Effects in Linear Scanline Results. *AAPG Bulletin*, 99(12): 2203–2219. https://doi.org/10.1306/05211514104

Sava, D., Mavko, G., 2007. Rock Physics-Based Integration of Geologic and Geophysical Data for Fracture Characterization. *The Leading Edge*, 26(9): 1140–1146. https://doi.org/10.1190/1.2780784

Su, Y., Zha, M., Ding, X. J., et al., 2018. Pore Type and Pore Size Distribution of Tight Reservoirs in the Permian Lucaogou Formation of the Jimsar Sag, Junggar Basin, NW China. *Marine and Petroleum Geology*, 89: 761–774. https://doi.org/10.1016/j.marpetgeo.2017.11.014

Tang, Y. Q., Wang, R., Li, Z. H., et al., 2019. Experimental Study on Spontaneous Imbibition of CO_2-Rich Brine in Tight Oil Reservoirs. *Energy & Fuels*, 33(8): 7604–7613. https://doi.org/10.1021/acs.energyfuels.9b01621

Wang, K., Liu, H., Luo, J., et al., 2017. A Comprehensive Model Coupling Embedded Discrete Fractures, Multiple Interacting Continua, and Geomechanics in Shale Gas Reservoirs with Multiscale Fractures. *Energy & Fuels*, 31(8): 7758–7776. https://doi.org/10.1021/acs.energyfuels.7b00394

Wang, X. F., Yang, Z. J., Yates, J. R., et al., 2015. Monte Carlo Simulations of Mesoscale Fracture Modelling of Concrete with Random Aggregates and Pores. *Construction and Building Materials*, 75: 35–45. https://doi.org/10.1016/j.conbuildmat.2014.09.069

Wei, Y. J., Anand, L., 2008. On Micro-Cracking, Inelastic Dilatancy, and the Brittle-Ductile Transition in Compact Rocks: A Micro-Mechanical Study. *International Journal of Solids and Structures*, 45(10): 2785–2798. https://doi.org/10.1016/j.ijsolstr.2007.11.028

Wu, H. G., Hu, W. X., Cao, J., et al., 2016. A Unique Lacustrine Mixed Dolomitic-Clastic Sequence for Tight Oil Reservoir within the Middle Permian Lucaogou Formation of the Junggar Basin, NW China: Reservoir Characteristics and Origin. *Marine and Petroleum Geology*, 76: 115–132. https://doi.org/10.1016/j.marpetgeo.2016.05.007

Wu, H. Q., Pollard, D. D., 2002. Imaging 3-D Fracture Networks around Boreholes. *AAPG Bulletin*, 86(4): 593–604. https://doi.org/10.1306/61eedb52-173e-11d7-8645000102c1865d

Wu, L. Y., Pang, X. Q., Zhou, L. M., et al., 2015. The Quality Evaluation and Hydrocarbon Generation and Expulsion Characteristics of Permian Lucaogou Formation Source Rocks in Jimusar Sag, Junggar Basin. *Acta Geologica Sinica (English Edition)*, 89(S1): 283–286. https://doi.org/10.1111/1755-6724.12304_29

Xi, K. L., Cao, Y. C., Jahren, J., et al., 2015a. Diagenesis and Reservoir Quality of the Lower Cretaceous Quantou Formation Tight Sandstones in the Southern Songliao Basin, China. *Sedimentary Geology*, 330: 90–107.

https://doi.org/10.1016/j.sedgeo.2015.10.007

Xi, K. L., Cao, Y. C., Zhu, R. K., et al., 2015b. Rock Types and Characteristics of Tight Oil Reservoir in Permian Lucaogou Formation, Jimsar Sag. *Acta Pharmacologica Sinica*, 36(12): 1495–1507 (in Chinese with English Abstract)

Yang, Y. Q., Qiu, L. W., Cao, Y. C., et al., 2017. Reservoir Quality and Diagenesis of the Permian Lucaogou Formation Tight Carbonates in Jimsar Sag, Junggar Basin, West China. *Journal of Earth Science*, 28(6): 1032–1046. https://doi.org/10.1007/s12583-016-0931-6

Yang, Z., Hou, L. H., Tao, S. Z., et al., 2015. Formation Conditions and "Sweet Spot" Evaluation of Tight Oil and Shale Oil. *Petroleum Exploration and Development*, 42(5): 555–565

Yuan, G. H., Gluyas, J., Cao, Y. C., et al., 2015. Diagenesis and Reservoir Quality Evolution of the Eocene Sandstones in the Northern Dongying Sag, Bohai Bay Basin, East China. *Marine and Petroleum Geology*, 62: 77–89. https://doi.org/10.1016/j.marpetgeo.2015.01.006

Zeng, L. B., 2010. Microfracturing in the Upper Triassic Sichuan Basin Tight-Gas Sandstones: Tectonic, Overpressure, and Diagenetic Origins. *AAPG Bulletin*, 94(12): 1811–1825. https://doi.org/10.1306/06301009191

Zeng, L. B., 2008. Formation and Distribution of Fractures in Low-Permeability Sandstone Reservoirs. Science Press House, Beijing. 1–169 (in Chinese)

Zeng, L. B., Gao, C. Y., Qi, J. F., et al., 2008a. The Distribution Rule and Seepage Effect of the Fractures in the Ultra-Low Permeability Sandstone Reservoir in East Gansu Province, Ordos Basin. *Science in China Series D: Earth Sciences*, 51(2): 44–52. https://doi.org/10.1007/s11430-008-6015-8

Zeng, L. B., Qi, J. F., Wang, C. G., et al., 2008b. The Influence of Tectonic Stress on Fracture Formation and Fluid Flow. *Earth Science Frontiers*, 15(3): 292–298 (in Chinese with English Abstract)

Zeng, L. B., Jiang, J. W., Yang, Y. L., 2010a. Fractures in the Low Porosity and Ultra-Low Permeability Glutenite Reservoirs: A Case Study of the Late Eocene Hetaoyuan Formation in the Anpeng Oilfield, Nanxiang Basin, China. *Marine and Petroleum Geology*, 27(7): 1642–1650. https://doi.org/10.1016/j.marpetgeo.2010.03.009

Zeng, L. B., Ke, S. Z., Liu, Y., 2010b. Fracture Study Methods for Low Permeability Oil and Gas Reservoir. Petroleum Industry Press, Beijing. 1–187 (in Chinese)

Zeng, L. B., Li, X. Y., 2009. Fractures in Sandstone Reservoirs with Ultra-Low Permeability: A Case Study of the Upper Triassic Yanchang Formation in the Ordos Basin, China. *AAPG Bulletin*, 93(4): 461–477. https://doi.org/10.1306/09240808047

Zeng, L. B., Li, Z. X., Shi, C. E., et al., 2007. Characteristics and Origin of Fractures in the Extra Low-Permeability Sandstone Reservoirs of the Upper Triassic Yanchang Formation in the Ordos Basin. *Acta Geologica Sinica*, 81(2): 174–180 (in Chinese with English Abstract)

Zeng, L. B., Su, H., Tang, X. M., et al., 2013. Fractured Tight Sandstone Oil and Gas Reservoirs: A New Play Type in the Dongpu Depression, Bohai Bay Basin, China. *AAPG Bulletin*, 97(3): 363–377. https://doi.org/10.1306/09121212057

Zeng, L. B., Tang, X. M., Wang, T. C., et al., 2012. The Influence of Fracture Cements in Tight Paleogene Saline Lacustrine Carbonate Reservoirs, Western Qaidam Basin, Northwest China. *AAPG Bulletin*, 96(11): 2003–2017. https://doi.org/10.1306/04181211090

Zha, M., Su, Y., Gao, C. H., et al., 2017. Tight Reservoir Space Characteristics and Controlling Factors: An Example from Permian Lucaogou Formation in Jimsar Sag, Junggar Basin, Northwest China. *Journal of China University of Mining and Technology*, 46(1): 91–101.

https://doi.org/10.13247/j.cnki.jcumt.000553 (in Chinese with English Abstract)

Zhang, C., Zhu, D. Y., Luo, Q., et al., 2017. Major Factors Controlling Fracture Development in the Middle Permian Lucaogou Formation Tight Oil Reservoir, Junggar Basin, NW China. *Journal of Asian Earth Sciences*, 146: 279–295. https://doi.org/10.1016/j.jseaes.2017.04.032

Zhang, J. L., He, S., Wang, Y. Q., et al., 2019. Main Mechanism for Generating Overpressure in the Paleogene Source Rock Series of the Chezhen Depression, Bohai Bay Basin, China. *Journal of Earth Science*, 30(4): 775–787. https://doi.org/10.1007/s12583-017-0959-6

Zhang, Y. Z., Zeng, L. B., Luo, Q., et al., 2020. Effects of Diagenesis on Natural Fractures in Tight Oil Reservoirs: A Case Study of the Permian Lucaogou Formation in Jimusar Sag, Junggar Basin, NW China. *Geological Journal*, 55(9): 6562–6579. https://doi.org/10.1002/gj.3822

Zhang, Y. Z., Zeng, L. B., Luo, Q., et al., 2018. Research on the Types and Genetic Mechanisms of Tight Reservoir in the Lucaogou Formation in Jimusar Sag, Junggar Basin. *Natural Gas Geoscience*, 29(2): 211–225 (in Chinese with English Abstract)

Zhao, J. M., Chen, S. Z., Deng, G., et al., 2019. Basement Structure and Properties of the Western Junggar Basin, China. *Journal of Earth Science*, 30(2): 223–235. https://doi.org/10.1007/s12583-018-1207-4

Zhao, P. Q., Wang, Z. L., Sun, Z. C., et al., 2017. Investigation on the Pore Structure and Multifractal Characteristics of Tight Oil Reservoirs Using NMR Measurements: Permian Lucaogou Formation in Jimusaer Sag, Junggar Basin. *Marine and Petroleum Geology*, 86: 1067–1081. https://doi.org/10.1016/j.marpetgeo.2017.07.011

Zhou, W. D., Xie, S. Y., Bao, Z. Y., et al., 2019. Chemical Compositions and Distribution Characteristics of Cements in Longmaxi Formation Shales, Southwest China. *Journal of Earth Science*, 30(5): 879–892. https://doi.org/10.1007/s12583-019-1013-7

Zhu, R. K., Zou, C. N., Mao, Z. G., et al., 2019. Characteristics and Distribution of Continental Tight Oil in China. *Journal of Asian Earth Sciences*, 178: 37–51. https://doi.org/10.1016/j.jseaes.2018.07.020

Zou, C. N., Guo, Q., Yang, Z., et al., 2019. Resource Potential and Core Area Prediction of Lacustrine Tight Oil: The Triassic Yanchang Formation in Ordos Basin, China. *AAPG Bulletin*, 103(6): 1493–1523. https://doi.org/10.1306/11211816511

Zou, C. N., Zhu, R. K., Wu, S. T., et al., 2012. Characteristics, Genesis and Prospects of Conventional and Unconventional Hydrocarbon Accumulations: Taking Tight Oil and Tight Gas in China as an Instance. *Acta Petrolei Sinica*, 33(2): 173–187 (in Chinese with English Abstract)